THE ASTROPHYSICAL JOURNAL SUPPLEMENT SERIES, 39:481–511, 1979 April

AN ATLAS OF THEORETICAL P CYGNI PROFILES

JOHN I. CASTOR AND HENNY J. G. L. M. LAMERS*
Joint Institute for Laboratory Astrophysics, National Bureau of Standards and University of Colorado
Received 1978 July 14; accepted 1978 October 4

ABSTRACT

An atlas of theoretical P Cygni–type line profiles is presented. The profiles are calculated assuming resonance scattering and using the Sobolev approximation. The expanding envelope is characterized by two functions; the optical depth $\tau(v)$ and the velocity law $v(r)$. The velocity law, the process of line formation, and the accuracy of the theoretical line profiles are discussed. The effect of collisional excitation is discussed and is found not to be important in most UV resonance lines, except in a star with a very high rate of mass loss and a small wind velocity. We describe a simple procedure to correct for the presence of underlying photospheric profiles, and show that the simple addition of the calculated P Cygni profile and photospheric profile can give very wrong results. We also describe a fairly simple procedure for calculating the shape of partly overlapping doublet lines. The accuracy of the information that can be derived from a comparison between observed and theoretical P Cygni profiles is discussed critically.

Subject headings: line formation — line profiles — stars: emission-line

I. INTRODUCTION

The ultraviolet spectra of luminous early-type stars exhibit line profiles consisting of a shortward displaced absorption component and a longward displaced emission component. These profiles are generally called P Cygni profiles. Beals (1951) has classified eight types of P Cygni profile on the basis of different wavelength shifts and of the ratio of the emission component to the absorption component. The profiles observed in the ultraviolet spectra of hot stars are called type I by Beals.

The interpretation of these profiles in terms of a spherically symmetric expanding shell or envelope was already understood in 1929 by McCrea (1929) and Beals (1929). In the simplest explanation the star is surrounded by an expanding shell that is optically thick at the wavelength of the line in the comoving frame. The part of the shell that is projected against the stellar disk moves toward the observer and produces a violet-shifted absorption. The part of the shell that is projected against the sky background surrounding the disk produces a wide emission, centered at zero velocity. The combination of these two components results in a P Cygni profile of type I. The exact shape of the profile will depend, of course, on the geometry of the expanding envelope; the velocity and velocity gradients in the envelope; the density of the absorbing particles; and the nature of the emission and absorption processes.

The study of the ultraviolet P Cygni profiles is the major source of information on the mass-loss rates of early-type stars and the structure of their expanding envelopes. (The radio fluxes can be used to determine the mass-loss rates accurately, but the observations are limited to only a very small number of the brightest stars. The infrared fluxes up to 22 μm also give information on the mass-loss rate, but since these fluxes arise from regions very close to the star with small velocities, they do not give information on the structure of the major part of the envelope.) Profiles of ultraviolet lines in about 60 early-type stars observed by the *Copernicus* satellite have been published by Snow and Morton (1976) and Snow and Jenkins (1977); the forthcoming observations by the *International Ultraviolet Explorer* will extend this number dramatically.

The observed profiles can be compared with predicted profiles if the physical characteristics of the model envelopes are known. Such a comparison could result in a refinement or adjustment of the model. However, our understanding of the structure of expanding envelopes of early-type stars—the velocity-radius relation, the temperature, and the ionization balance—is still very poor. Therefore, we adopt a more fruitful approach of calculating theoretical P Cygni profiles for a grid of simplified model envelopes, which later can be compared with the observations to derive the gross characteristics of the envelopes. This method was applied earlier by Lamers and Morton (1976) and Lamers and Rogerson (1978) in their studies of ζ Pup (O4f) and τ Sco (B0 V), and by Olson (1978) in his study of ζ Pup.

In §§ II and III the assumptions and the philosophy of selecting the parameters will be discussed. The transfer equation is solved for a spherically symmetric expanding envelope by adopting the Sobolev approximation. This approximation is valid if the velocity gradient is so large that the scale length for the density and temperature variations in the envelope is much larger than the length in which the expansion velocity increases by the thermal velocity. The numerical

* On leave of absence from the Space Research Laboratory of the Astronomical Institute at Utrecht.

method and the accuracy of the profiles are described in § III. The grid of profiles is presented in § IV, both numerically and in graphs. We discuss the sensitivity of the profiles to the model parameters and to the limb darkening, and we describe curves of growth for the absorption part of the profile as well as the ratio between emission and absorption. The effects of an underlying photospheric absorption line are discussed in § V, the influence of collisional excitation on the profile is considered in § VI, and the effects of overlapping doublet lines are investigated in § VII. Section VIII offers some conclusions about what may be learned from a comparison of the profiles with observations and mentions pitfalls to be avoided in this process.

II. THE MODEL ENVELOPES

a) *Choice of the Parameters*

The profiles and curves of growth presented in this paper are meant to be compared with observed profiles in order to obtain information on the structure of the expanding envelopes. This implies that we have to adopt model atmospheres that can be specified by a few parameters and still give a meaningful description of the real envelopes. Moreover, we want to choose these parameters in such a way that their influence on the line profiles is clearly defined, so that these parameters can be derived uniquely from the observations.

The actual parameters that determine a line profile are the radius of the star, the mass-loss rate, the velocity law, the fractional abundance of the absorbing ions, and the atomic parameters like wavelength and oscillator strength. The radius, mass-loss rate, wavelength, and oscillator strength can be considered as scaling factors of the line profile. Therefore, we might adopt the velocity law and the fractional abundance as a function of the distance from the star as the parameter for profiles. However, these two quantities enter the calculations of the line profiles in a coupled way via the optical depth scale.

The radial optical depth in an expanding envelope is given by

$$\tau_{\rm rad}(r) = \frac{\pi e^2}{mc} f \lambda_0 n_i \left(\frac{dr}{dv}\right) , \qquad (1)$$

where f is the absorption oscillator strength, λ_0 (in cm) is the rest wavelength of the transition, n_i (in cm^{-3}) is the number density of the absorbing ions at a distance r, and dr/dv (in s) is the inverse velocity gradient. The quantities n_i and dr/dv are evaluated at the radial distance r. We assume that the velocity increases monotonically with radius, so that dr/dv is uniquely defined. This $\tau_{\rm rad}$ is the total optical depth presented by the envelope to a photon traveling radially at that frequency which would be resonantly absorbed at radius r. Most of this optical depth is contributed by a thin shell across which $\Delta v \approx v_{\rm thermal}$.

Our models are specified by two functions: the radial optical depth as a function of the flow velocity, $\tau_{\rm rad}(v)$, and the velocity law of the envelope, $v(r)$. This approach may be contrasted with that of Olson (1978), who adopted the two functions $v(r)$ and n_i/ρ versus r as the basic ones for his parametric description. These descriptions are entirely equivalent since, given the velocity law, one can convert n_i/ρ into $\tau_{\rm rad}$ using equation (1) and the law of mass conservation. Thus the grids of profiles based on the two types of parametrization differ in the labeling of the profiles, not in their nature. If it were in fact possible to determine both of the functions from an observed profile, then the preferred parametrization would be entirely a matter of convenience; in that case Olson's scheme might be better since it is more closely tied to the physical structure of the envelope. As we will discuss at some length below, the determination of both functions is not likely to be possible in practice. One will have to *guess* one of the functions, then use the observed profile to derive the other. In this case it makes sense to parametrize the problem such that the function that is derived is not too sensitive to the function that must be guessed. In our opinion, this is the virtue of using $\tau_{\rm rad}(v)$; we will show in § IV*a* that the absorption part of the profile depends very strongly on $\tau_{\rm rad}(v)$ and only very little on $v(r)$. The emission part of the profile depends on both functions but depends in addition on the underlying photospheric absorption, which is not well known.

b) *Velocity Law: v*(*r*)

The model envelope is assumed to be spherically symmetric and expanding. The expansion velocity $v(r)$ increases monotonically outward and asymptotically approaches a terminal velocity v_∞ at very large distances. Such a velocity structure is suggested by the profiles of the UV resonance lines in luminous O and B stars and in A-type supergiants. In those stars that have a high mass-loss rate, the strongest UV lines show P Cygni profiles with a steep edge on the short-wavelength side of the absorption component and this edge velocity is about the same for all the strong lines in a given star (Snow and Morton 1976; Lamers, Stalio, and Kondo 1978).

We normalize all velocities to the terminal velocity by defining a normalized velocity

$$w = v/v_\infty \, . \qquad (2)$$

Similarly, the distance r from the stellar center will be normalized by

$$x = r/R_* \, , \qquad (3)$$

where R_* is the photospheric radius, so that $x > 1$ in the envelope.

The exact shape of the velocity law $w(x)$ in early-type stars is unknown. Castor, Abbott, and Klein (1975) have predicted a very steep velocity law for a radiation-driven stellar wind model. Abbott (1977) has refined these theoretical calculations by taking into account a more realistic method for the calculation of the line radiation pressure, which includes about 3×10^4 lines.

He finds two velocity laws which have to be considered as extremes that bracket the real velocity law. The soft velocity law (slowly increasing with distance) was found by including a maximum of line blending; i.e., photons that are scattered by one line contribute negligibly to the net force when they are subsequently scattered in another spectral line. The steep velocity law includes no effect of blending; i.e., the photons are scattered in each line just as if they had suffered no previous scatterings by other lines. Lamers and Morton (1976) derived a velocity law from the profiles of the UV resonance lines in ζ Pup which is between the two extreme laws predicted by Abbott. Barlow and Cohen (1977) derived a very soft velocity law from the observed radio and infrared spectrum of P Cyg by assuming that the infrared excess is due to free-free emission in the expanding envelope. Cassinelli, Olson, and Stalio (1978) derived a velocity law from the Hα profile in ζ Ori that includes a plateau at 400 km s^{-1} near $r \approx 1.5\, R_*$. The plateau was required in order to produce an absorption component at -300 km s^{-1}. The rapid rise from the plateau to the terminal velocity of 2250 km s^{-1} suppressed emission from the higher-velocity material, not observed in the profile. (The wavelength error of 4 Å in the Cassinelli *et al.* profile, pointed out by Ebbets 1977, has only a small effect on these conclusions.) Hutchings (1970, 1977) derived velocity laws from the UV resonance lines of supergiants and found a difference between the velocity law for Orion stars and for other supergiants, but he does not give sufficient details to compare them with other velocity laws. Conti (1978) tried to derive a velocity law from the X-ray luminosity of three X-ray binaries that are powered by accretion from the wind, using the method of Lamers, van den Heuvel, and Petterson (1976), but did not find a satisfactory solution owing to the uncertainties in the models.

These velocity laws are shown in Figure 1*a* in terms of w versus $1/x$. The enormous difference between the various laws is distressing, and one can conclude only that either there is no unique velocity law for all the early-type stars or the true velocity law is still unknown.

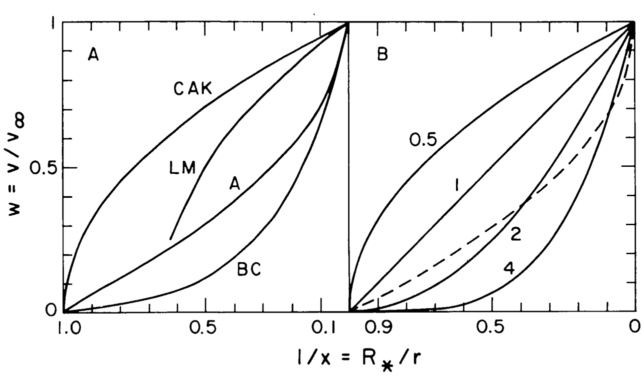

FIG. 1.—(*a*) Observed and theoretical velocity laws are labeled according to their authors: CAK (Castor, Abbott, and Klein 1975), LM (Lamers and Morton 1976), A (Abbott 1977, maximum blending), BC (Barlow and Cohen 1977). (*b*) The velocity laws adopted in this study described by eq. (4) and labeled with the value of β are shown by solid lines. The velocity law of eq. (5) is given by a dashed line.

Therefore, we have chosen for our models a simple analytical expression for the velocity law of the type

$$w = 0.01 + 0.99(1 - 1/x)^\beta \tag{4}$$

with $\beta > 0$. This law ensures that $w = 1$ at very large distances from the star and w is small at the photosphere $x = 1$. The value of $w(x = 1) = 0.01$ would correspond to a flow velocity of about 25 km s^{-1} at the base of the wind. This agrees reasonably well with the mean expansion velocity (based on several moderate-strength lines) of 29 km s^{-1} found in Of stars by Conti, Leep, and Lorre (1977). We point out, however, that the exact value of $w(x = 1)$ has little importance for the profiles of the UV resonance lines.

The values of β that we have chosen for this study are $\beta = 0.5$, 1, 2, and 4. The corresponding velocity laws shown in Figure 1*b* can be compared with those in Figure 1*a*. We notice that the curve for $\beta = 0.5$ is identical to the theoretical law of Castor *et al.* and the hard velocity law of Abbott. The curve for $\beta = 1$ resembles the velocity law derived by Lamers and Morton for ζ Pup for $w > 0.5$, whereas the curve for $\beta = 4$ resembles Barlow and Cohen's velocity law for P Cyg. Abbott's soft velocity law is represented fairly accurately by

$$w = 0.03 + 0.97(1 - 1/\sqrt{x})\,, \tag{5}$$

which is also shown in Figure 1*b*.

We will show later that the absorption part of the calculated P Cygni profiles depends very little on the adopted velocity law.

c) Optical Depth Law: $\tau(w)$

The variation of optical depth with velocity depends on the variations of ion density and velocity gradient (eq. [1]). In order to adopt reasonable $\tau(w)$ functions, we need to consider the expected change of ionization balance in the envelopes. Of course, we do not know *a priori* what the ionization balance is, since that is one of the things we expect to determine from the profile fitting. The best we can do is to consider some possible models of ionization balance and choose a parametrization for $\tau(w)$ that easily accommodates these. We need to keep in mind that no simple formula for $\tau(w)$ can possibly account exactly for the variation in abundance of an actual ion.

For our first choice of the form for $\tau(w)$ we are guided by this simple model of ionization balance: photoionization by the diluted stellar continuum radiation to which the envelope is supposed to be optically thin. On this model the ionization ratio for successive stages is proportional to W/n_e, where W is the dilution factor. The result is that the ionization ratio is proportional to w, and the individual ion abundances vary as powers of w provided the dominant ion is the same throughout the wind. In conjunction with mass conservation and equation (4) for the velocity law, this implies that $\tau(w)$ should vary as a power of w:

$$\tau(w) \propto w^\alpha\,. \tag{6}$$

The profiles calculated with $\tau \propto w^{\alpha}$ have a residual intensity in the violet wing of $\exp[-\tau(w = 1)]$ at $w = -1$ (see Fig. 4*a*). The profiles of the UV resonance lines observed by Snow and Morton (1976), however, show either a steep violet edge if the lines are very strong, or an absorption wing that gradually approaches the continuum if the lines are weak. This indicates that either the velocity law is different from the ones described by equation (4), or the ionization does not follow the model above, or both. Lamers and Morton (1976) have pointed out that the profiles of the UV resonance lines of ζ Pup can be described very well by a relation of the type $\tau \propto 1 - w$.

We have accommodated the optical depth law suggested by equation (6), as well as the indications that $\tau_{\rm rad} \propto 1 - w$ might be better, by computing two sets of profiles. For one set we use

$$\tau_{\rm rad}(w) = \mathscr{T}(\alpha + 1)(1 - w_0^{\alpha+1})^{-1}w^{\alpha} \tag{7a}$$

if $\alpha \neq -1$, and

$$\tau_{\rm rad}(w) = -\mathscr{T}(\ln w_0)^{-1}w^{-1} \tag{7b}$$

if $\alpha = -1$. For the other set we adopt the law

$$\tau_{\rm rad}(w) = \mathscr{T}(\gamma + 1)(1 - w_0)^{-1-\gamma}(1 - w)^{\gamma} \tag{8}$$

with $\gamma \geq 0$. We take $w_0 = 0.01$ for the flow speed at the base of the envelope. The quantity $\mathscr{T}$ is related to the total optical depth and is given by

$$\mathscr{T} = \int_{w_{\rm phot}}^{1} \tau_{\rm rad}(w)dw = \frac{\pi e^2}{mc}\frac{f\lambda_0}{v_\infty}N_i\,, \tag{9}$$

where N_i is the column density (cm^{-2}) of the absorbing ion in the envelope. The product $\mathscr{T}v_\infty$ is proportional to N_i, and we will use it as a curve-of-growth parameter.

III. CALCULATION OF THE PROFILES

a) *Process of Line Formation*

Most of our computed profiles assume conservative scattering. The probability of destruction of a photon and the corresponding rate of creation of photons are small, as we can see by computing

$$\epsilon = \frac{n_e C_{21}}{A_{21}}\left[1 - \exp\left(-\frac{\chi_{12}}{kT_e}\right)\right] \tag{10}$$

and

$$\eta = \frac{R_{2k}}{A_{21}}\,, \tag{11}$$

where $n_e C_{21}$ is the rate of collisional de-excitation and R_{2k} is the rate of photoionization, both per excited ion. With van Regemorter's (1962) approximation for C_{21} we find

$$\epsilon \approx 6.2T_e^{-1/2}n_e\lambda^3\left[1 - \exp\left(-\frac{\chi_{12}}{kT_e}\right)\right]\,. \tag{12}$$

Electron densities in the high-velocity part of the wind ($w \gtrsim 0.5$) range from 10^8 to 10^{11} cm^{-3}, with the result that ϵ ranges from less than 10^{-8} to 10^{-5}. The value of η depends strongly on the photoionizing radiation field, but if we assume $J_\nu \approx WB_\nu(T_*)$, then

$$\eta \approx 9.45 \times 10^{-3}W\frac{a_{18}}{f_{21}}\lambda_{1000}{}^2\left(\frac{\chi_2}{I_{\rm H}}\right)^2(T_*)_4 \times \exp(-\chi_2/kT_*)\,, \tag{13}$$

where a_{18} is the photoionization cross section of level 2 in 10^{-18} cm^2, f_{21} is the emission oscillator strength, λ_{1000} is the wavelength of the 2–1 transition in units of 1000 Å, χ_2 is the ionization potential of level 2, $I_{\rm H}$ is the ionization potential of hydrogen, and $(T_*)_4$ is T_* in units of 10^4 K. With $T_* \lesssim 4 \times 10^4$ K, $\chi_2 \gtrsim 40$ eV, and $W \lesssim 0.5$, we find that $\eta \lesssim 3 \times 10^{-5}$.

The effect of ϵ or η is negligible unless

$$\epsilon\tau > \frac{WI_c}{B_\nu}$$

or

$$\eta\tau > \frac{WI_c}{B^*}$$

(see Castor 1970). In these expressions I_c is the intensity of the photosphere at the line frequency, B_ν is the Planck function at the electron temperature, and $B^* \approx B_\nu(T_*)$. For a line at 1000 Å, with $T_e \lesssim 2 \times 10^5$ K and $T_* \gtrsim 2.5 \times 10^4$ K, $I_c/B_\nu \gtrsim 10^{-2}$. We may suppose that $B^* \approx I_c$. Therefore, these effects are not important unless τ is very large ($\tau \gtrsim 10^3$).

The effect of ϵ on profiles for very optically thick lines will be illustrated in § VI.

We assumed complete frequency redistribution for the scattering process. Mihalas, Kunasz, and Hummer (1976) showed that the assumption of complete frequency redistribution gives an accurate approximation to the source function of the lines in a moving atmosphere. They found that even if the lines have a coherent scattering wing, the assumption of complete redistribution is still to be preferred to coherent scattering for the line as a whole provided that the optical thickness is not too large.

The majority of the resonance lines are doublets whose components overlap in the emergent spectrum. This overlap alters the line source functions and considerably modifies the profiles. This problem is taken up in § VII.

b) *Method of Calculation*

The profiles of the single resonance lines without thermal emission were calculated with a method developed by Lucy (1971). The profiles with thermal emission and those of doublets were calculated with the escape probability method of Castor (1970). Both methods employ the Sobolev approximation, which neglects the intrinsic line width relative to the Doppler displacements. In Lucy's method the angular dependence of the intensity is approximated by two streams with a properly chosen boundary between them. In Castor's method the angular dependence is treated exactly, using escape probabilities. The radius of the envelope was taken as the larger of 10^3 stellar radii and the radius where $w = 0.99$. The computations were done with the CDC 6400 computer of the University of Colorado in Boulder. A typical line profile, calculated at 46 frequencies, takes about 18 s computer time at a cost of about $0.50 per profile.

c) Accuracy of the Profiles

In order to estimate the accuracy of the calculations, we compared a series of profiles calculated with Lucy's method and Castor's method ($\epsilon = 0$). We found that the profiles agree within 1%, except near the line center of a profile with $\tau = 1$, where the intensity predicted by the escape probability method was 2.5% higher than that predicted by Lucy's method. So the two methods, both of which assume the Sobolev approximation, agree very well.

In order to estimate the effect of the Sobolev approximation, we have compared our profiles for a plane-parallel atmosphere with those derived by Noerdlinger and Rybicki (1974) from an accurate solution of the transfer equation in the moving medium. In order to make this comparison, we had to adopt a very thin envelope with a thickness of $\Delta R/R_* \approx 10^{-2}$ around a spherical star to make the envelope nearly planar. This comparison is shown in Figure 2, where the profiles computed by Noerdlinger and Rybicki are compared with our profiles for the same cases. We note that the agreement is better than 0.5% throughout the violet absorption wing, except within 2 Doppler widths of the line center. At such small velocities the thermal motions of the ions cannot be neglected and so the Sobolev approximation breaks down. We also compared some other profiles published by Noerdlinger and Rybicki with our calculations for similar cases, with the same results: a very good agreement for the absorption part, except within 2 Doppler widths from the line center.

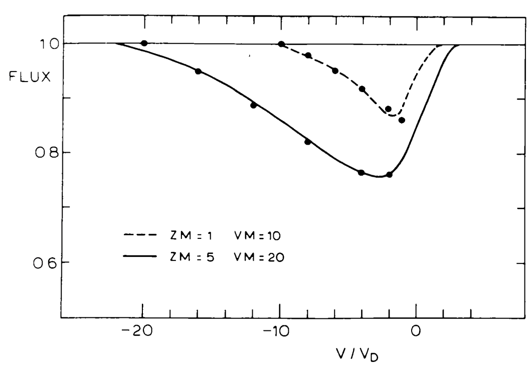

FIG. 2.—Comparison of profiles calculated with (*dots*) the Sobolev approximation and (*dashed and solid lines*) the modified Feautrier method in a plane-parallel atmosphere. The profiles are indicated by the values of ZM and VM (Noerdlinger and Rybicki 1974). [VM is the maximum expansion velocity in thermal units, $v_{\max}/v_{\text{th}}$, while ZM is a total optical depth related to our $\tau(w)$ by ZM = $\tau(w)$VM.] The profiles of the two methods agree within 0.5% with one another, except within 2 Doppler widths from the line center, where the Sobolev approximation breaks down.

The profiles for a plane-parallel atmosphere lack an emission component; we must consider a spherical extended atmosphere in order to obtain a true P Cygni line. Accurate calculations of line profiles in a rapidly expanding spherical envelope have been made only by Mihalas, Kunasz, and Hummer (1975). Unfortunately, the sample P Cygni profiles shown in that paper are for cases in which most of the continuum emission emanates from the outermost part of the envelope; while such a situation can be treated with the Sobolev approximation, it could not be done with the methods we have used in this paper. Therefore, we are unable to compare our method of calculation with a more accurate one for a spherical case. However, there is reason to think that the Sobolev approximation is better in spherical cases than in plane-parallel ones; this is indicated by the comparison of the exact and Sobolev source functions given by Mihalas, Kunasz, and Hummer (1975, Fig. 7).

From these comparisons we may conclude that our profiles are more accurate than about 1% of the continuum flux, except within 2 Doppler widths from the line center, where our profiles are wrong.

IV. PROFILES

a) Sensitivity of the Profiles to $\tau_{\text{rad}}(w)$ and $w(x)$

All profiles throughout this paper will be normalized in such a way that the continuum flux is 1. The wavelength scale will be expressed in radial velocity (Δw) normalized to $\Delta w = 0$ at the line center λ_0, and $\Delta w = +1$ at $\lambda = \lambda_0(1 + v_\infty/c)$.

The profiles for a few special cases are shown in Figures 3 and 4 in order to demonstrate the sensitivity of the profiles to various parameters. We assumed that the photosphere emits a continuum that is flat over the frequency range of the line profile, with no photospheric absorption line and no limb darkening. The effects of photospheric absorption and limb darkening will be discussed later.

Figure 3 shows profiles for the same $\tau_{\text{rad}}(w)$ relation but various velocity laws. We notice that the absorption parts of the profiles are very similar, despite the very large differences in the velocity laws. (See Fig. 1*b*.) On the other hand the emission component depends strongly on the velocity law. Figure 4 shows the profiles for the same velocity law and the same total optical depth $\mathcal{T}$, but with different values of α and γ (eqs. [7] and [8]), i.e., different density distributions of the ions through the envelope. These profiles differ strongly from one another in the shape of the absorption component as well as in the amount of emission. Figures 5–8 show the profiles for a given velocity law and a given value of α or γ, but with various values of $\mathcal{T}$; i.e., the density distributions of the ions are the same but differ by a constant factor, or the lines have

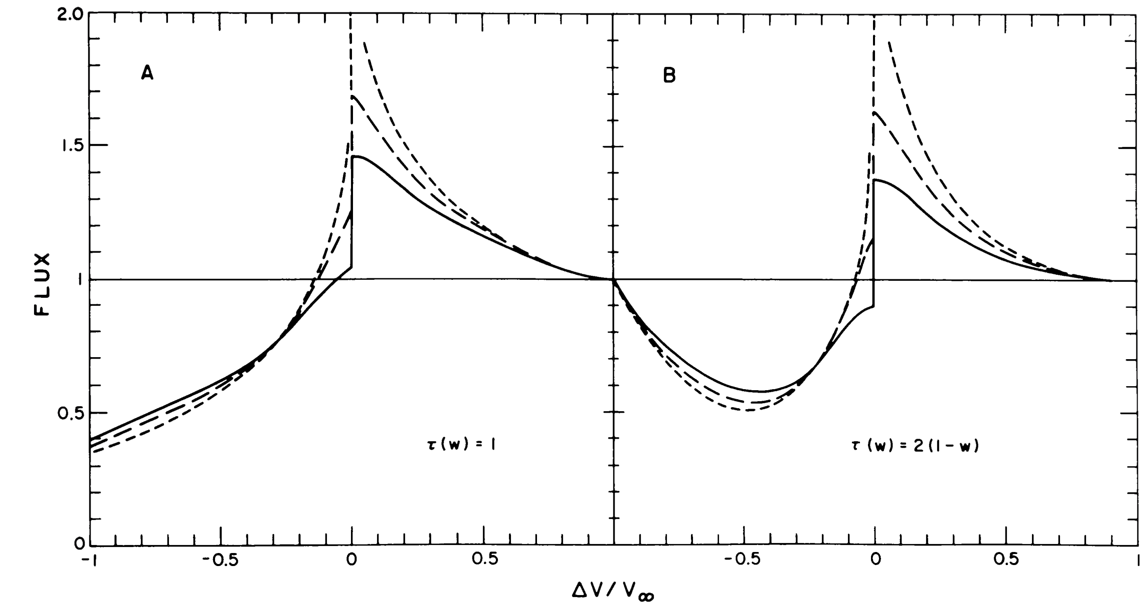

FIG. 3.—Sensitivity of the profiles to the velocity law. The profiles in the left panel are calculated with $\tau(w) = 1$, and those in the right panel with $\tau(w) = 2(1 - w)$. The velocity law is $w = 0.01 + 0.99[1 - (1/x)]^{\beta}$ with (*solid line*) $\beta = 0.5$, (*long-dashed line*) $\beta = 1$ and (*short-dashed line*) $\beta = 4$. Notice that the absorption part is very insensitive to the velocity law.

different oscillator strengths. We notice a strong dependence of the profiles on $\mathscr{T}$ in that the absorption and the emission components both increase with increasing $\mathscr{T}$.

From these comparisons we conclude that the profile of the absorption component depends very strongly on $\tau_{\rm rad}(w)$ but only very little on the velocity law. This conclusion was anticipated in § II*a*; in fact, this was the reason for choosing $\tau(w)$ as a parameter rather than $\tau(x)$. We also find that the emission component depends on $\tau(w)$ as well as $w(x)$ in that a slower velocity law produces a large emission.

In the limit of very optically thick lines, $\tau(w) \gtrsim 10^2$, the profiles are independent of $\tau(w)$ and depend only on the velocity law. We present these saturated profiles for a number of velocity laws in Figure 9.

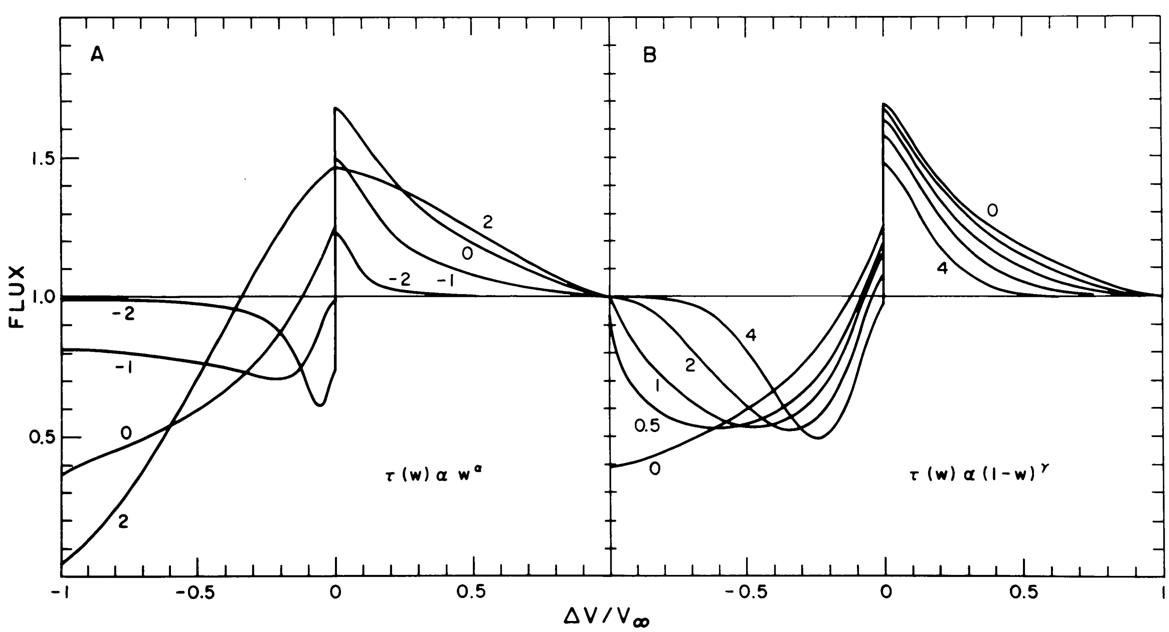

FIG. 4.—Sensitivity of the profiles to the optical depth law $\tau(w)$. All profiles are calculated with a velocity law of $w = 0.01 + 0.99[1 - (1/x)]$ and a total optical depth of $\mathscr{T} = 1$. The left-hand panel shows profiles for $\tau(w) \propto w^{\alpha}$, and the right-hand panel for $\tau(w) \propto (1 - w)^{\gamma}$. The parameters are α and γ, respectively.

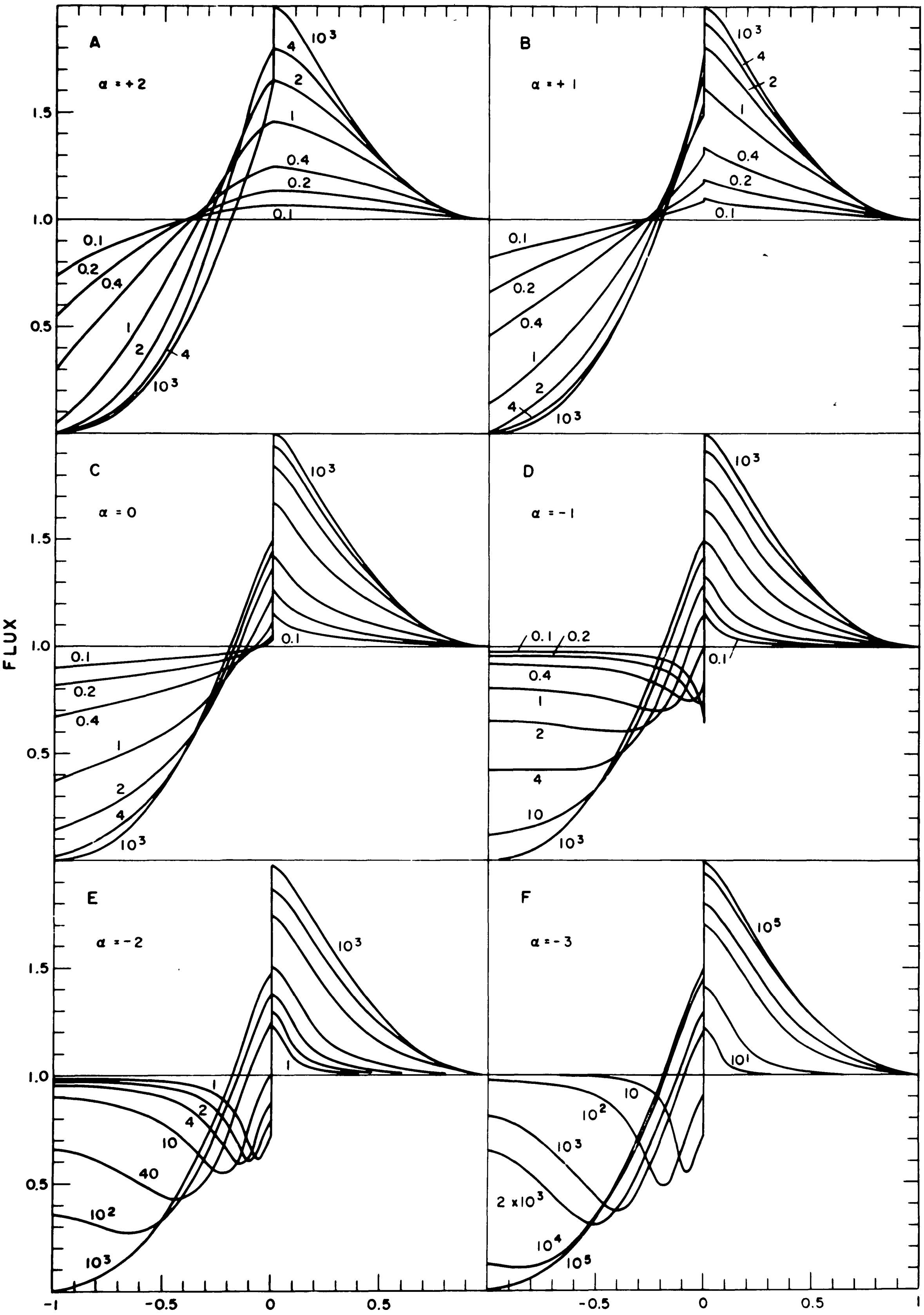

FIG. 5.—Profiles calculated with a velocity law of $w = 0.01 + 0.99[1 - (1/x)]$ and $\tau(w) \propto w^{\alpha}$. The six panels show profiles for various values of α. Within each panel the profiles are labeled by the total optical depth $\mathscr{T}$.

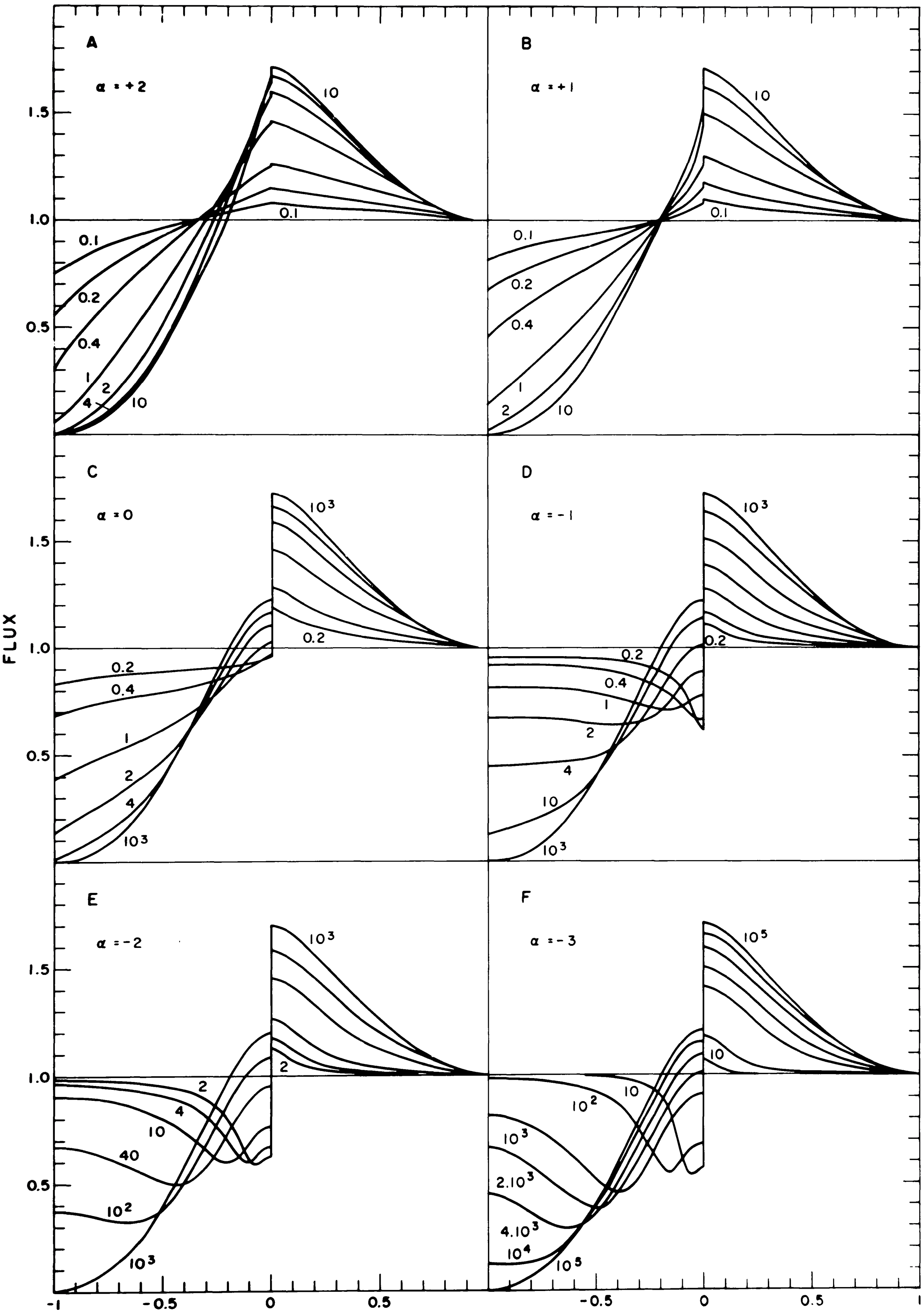

FIG. 6.—Same as Fig. 5, but with velocity law $w = 0.01 + 0.99[1 - (1/x)]^{0.5}$

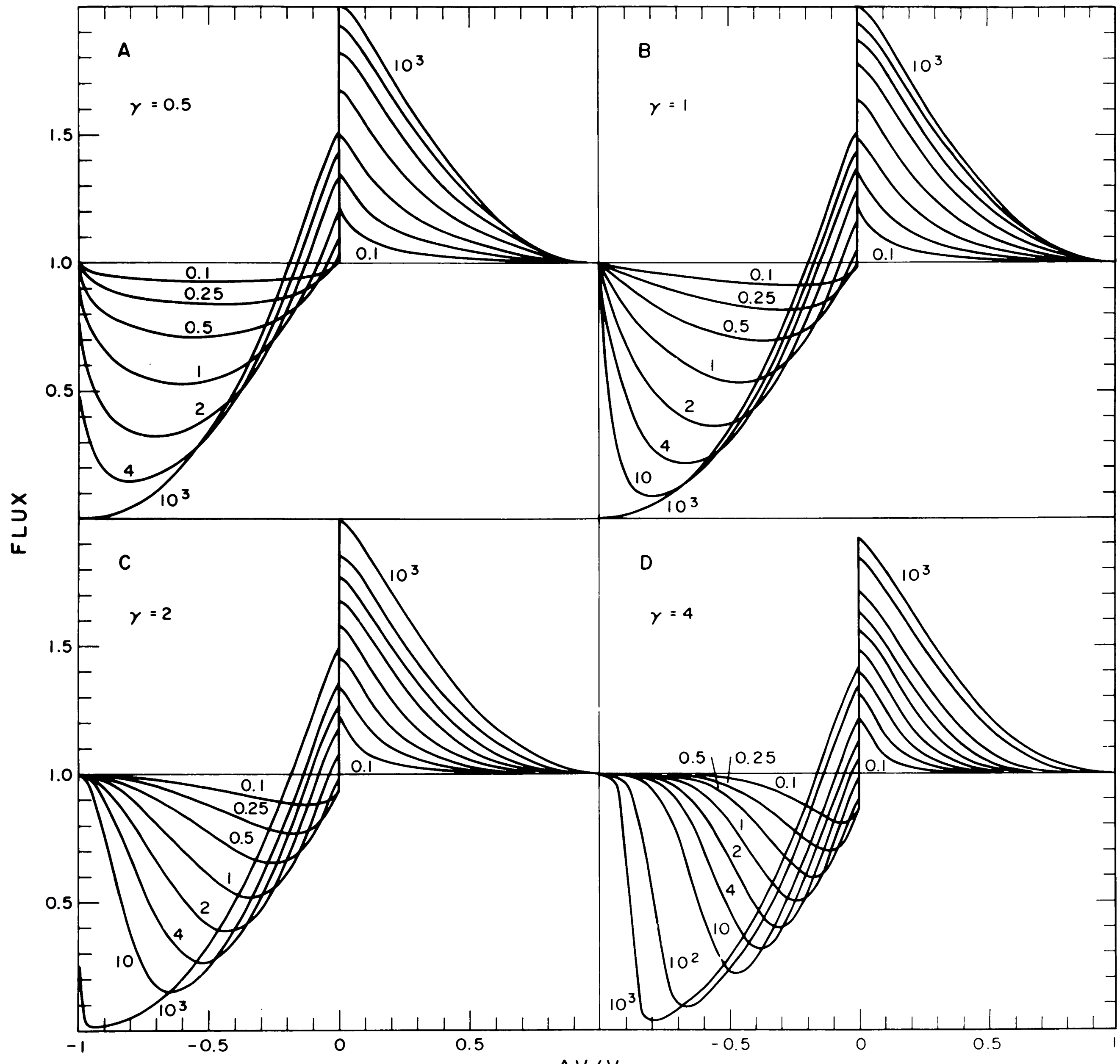

FIG. 7.—Profiles calculated with a velocity law of $w = 0.01 + 0.99[1 - (1/x)]$ and $\tau(w) \propto (1 - w)^{\gamma}$. The four panels show profiles for various values of γ. Within each panel the profiles are labeled by the total optical depth $\mathscr{T}$.

b) Limb Darkening

The profiles in this atlas are calculated with a photospheric continuum spectrum without limb darkening. In order to estimate the possible errors due to this assumption, a few profiles were calculated with limb darkening. The quadratic limb-darkening law

$$I_{\nu}(\mu) = I_{\nu}(0)(1 - U_1 - U_2) + U_1\mu + U_2\mu^2 \quad (14)$$

was adopted, where U_1 and U_2 are the limb-darkening factors and $\cos^{-1}(\mu)$ is the angle between the direction of radiation and the normal to the stellar surface. The profiles calculated with a mild ($U_1 = 0.60$, $U_2 = 0$) and a strong ($U_1 = 0$, $U_2 = 1.0$) limb darkening agree within 0.5% with those calculated without limb darkening, except very close to the line center, $|\Delta w| < 0.05$, where the difference can amount to 15%. So the effect of limb darkening is not important when observed profiles are compared with predicted profiles.

c) Atlas of Line Profiles

Figures 5–8 show the profiles of resonance lines formed by pure scattering ($\epsilon = 0$) for several velocity

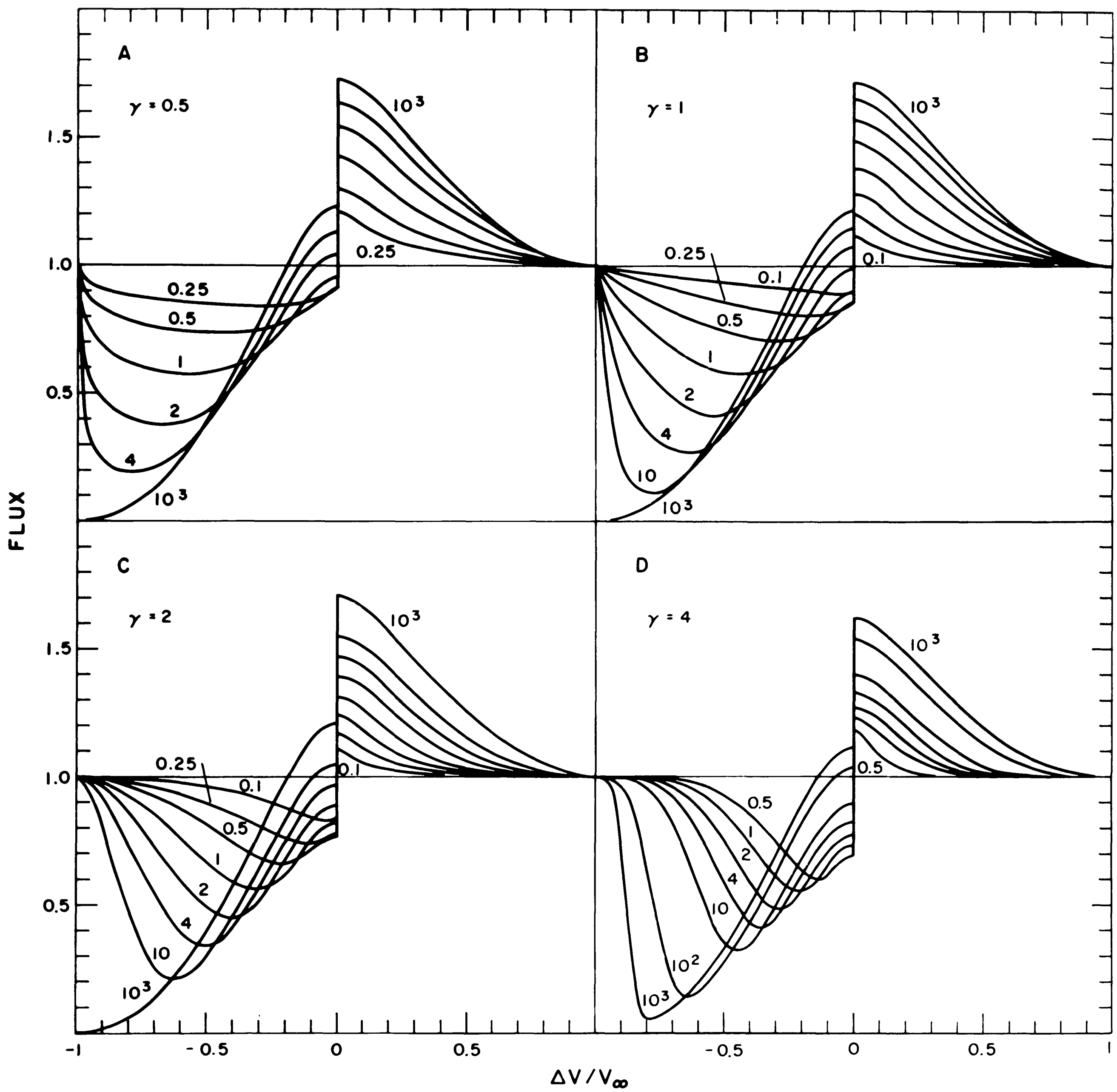

FIG. 8.—Same as Fig. 7, but with velocity law $w = 0.01 + 0.99[1 - (1/x)]^{0.5}$

laws and different values of the total optical depth $\mathscr{T}$ and α or γ (eqs. [7], [8], and [9]). The profiles are given in numerical form in Tables 1–6. The tables also list the values of the total equivalent width W_T (absorption minus emission), the equivalent width of the short-wavelength part ($\Delta w < 0$) of the profile W_B, the equivalent width of the long-wavelength part of the profile W_R, and the ratio W_R/W_B.

The effect on the profile of the absence of the ion ($\tau = 0$) in part of the envelope is shown in Figure 10 and Table 6. For these profiles we adopted

$$\tau_{\rm rad}(w) = \mathscr{T}(\gamma + 1)(w_{\rm max} - w)^{\gamma}(w_{\rm max} - w_{\rm min})^{-\gamma-1}, \tag{15}$$

which gives $\tau \neq 0$ only for $w_{\rm min} < w \leq w_{\rm max}$. For $w_{\rm max} = 1$ and $w_{\rm min} = w_0$, this equation reduces to equation (8). We considered values of $(w_{\rm min}, w_{\rm max}) = (0.01, 0.5)$ and $(0.5, 1.0)$.

d) *Scaling of the Profiles*

The profiles are presented in terms of flux normalized to the continuum versus radial velocity normalized to the terminal velocity. So in order to compare these profiles with the observations, the abscissa has to be multiplied by the terminal velocity. If a particular theoretical profile matches the observations, the

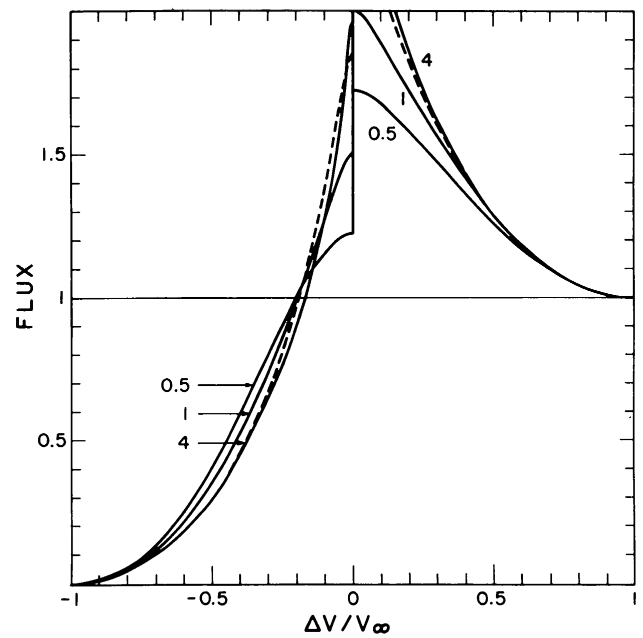

FIG. 9.—Profiles of fully saturated lines, which depend only on the velocity law. *Solid lines*, $v/v_\infty = 0.01 + 0.99[1 - (1/x)]^\beta$ with the value of β indicated. *Dashed line*, $v/v_\infty = 1 - x^{-1/2}$.

corresponding value of the product $n_i(dx/dw)$ can be derived from equation (1):

$$n_i(dx/dw) = \tau(w)\Big/\left(\frac{\pi e^2}{mc} f\lambda_0 \frac{R_*}{v_\infty}\right) . \quad (16)$$

So if the velocity law $w(x)$ or $v(r)$ is known, then the $n_i(r)$ can be derived or, alternatively, if $n_i(r)$ is known, then dw/dx or dv/dr can be derived from which the velocity law $v(r)$ can be determined. If the abundance and ionization fraction of the ion in question are known or can be found, the ion density $n_i(r)$ can be transformed into a mass density and the mass-loss rate can be derived.

e) *Curves of Growth*

In Figure 11 we show the curves of growth for the theoretical profiles, calculated with $\epsilon = 0$ and a non-truncated envelope. The ordinate shows the logarithm of the equivalent width of the short-wavelength side of the profile W_B expressed in units of the terminal velocity. This W_B is related to the conventional equivalent width W_λ in angstroms by

$$W_\lambda = W_B(\lambda_0 v_\infty/c) . \quad (17)$$

The abscissa shows the total optical depth $\mathscr{T}$, which is related to the conventional optical depth and the column density by equation (9). The curves of Figure 11 refer to the profiles with the velocity law of equation (4) and $\beta = 1$. However, the curves for $\beta = 0.5$ and $\beta = 4$ are very similar and differ at most by $\Delta \log W_B = 0.03$ at any value of $\mathscr{T}$. So these curves are almost independent of the velocity law.

The shape of the curves depends on the variation of $\tau(w)$, i.e., on α (eq. [7]) or γ (eq. [8]). The curves with constant τ ($\alpha = 0$ or $\gamma = 0$) show a linear part and a short transition to the saturation level. The curves with α or γ very different from 0 show a long transition between the linear part and saturation. For small values of $\mathscr{T}$ the curves of growth become linear:

$$\log W_B \approx \log \mathscr{T} - 0.25 . \quad (18)$$

(The linear part varies between $W_B = \mathscr{T}$ and $W_B = \mathscr{T}/2$ depending on the radial distribution of ion density.) By substituting the expressions for W_B and $\mathscr{T}$, we find that the linear part of the classical curve of growth for pure absorption would be given by $W_B = \mathscr{T}[2B_1/(2B_1 + 3B_0)]$, where $B_\nu = B_0 + B_1\tau_c$, if the Doppler velocity were equal to v_∞.

All curves reach their saturation level at $W_B = 0.50$, which means that for the strongest lines the entire flux between $\Delta v = 0$ and $\Delta v = -v_\infty$ is absorbed, but half of that is returned as emission on the short-wavelength side. The emission on the long-wavelength side is less than $-W_R = 0.5$ owing to the effect of the occulting stellar disk.

f) *Emission/Absorption Ratio*

The curves of growth, discussed above, depend little on the velocity law. An easy to measure parameter that does depend strongly on the velocity law is the ratio between the equivalent width of the long-wavelength side of the profile (emission) and the equivalent width of the short-wavelength side of the profile (absorption minus emission). This ratio is listed in Tables 1–5 for the calculated profiles and plotted in Figure 12 for the velocity law of equation (4) with $\beta = 0.5$, 1, and 4. Notice the strong dependence of the ratio on the velocity law for any optical depth law.

V. CORRECTING FOR PHOTOSPHERIC ABSORPTION LINES

In most of the ultraviolet resonance lines observed in the spectra of early-type stars, the P Cygni profiles are superposed on a photospheric absorption profile. In the analysis of such features it is often assumed that the resulting profile can be considered as a linear superposition of the photospheric and the envelope profiles, and the observed profiles are corrected for the photospheric profile accordingly (e.g., Cassinelli *et al.*). It is obvious, however, that the true interplay between photospheric and envelope lines is more complicated because the photospheric spectrum should be the lower boundary condition for the integration of the transfer equation in the moving envelope. The complication arises because at any point in the envelope the radiation along a ray from parts of the stellar disk has a Doppler shift that varies with the flow velocity in the envelope and the angle between the normal and the direction of the ray.

We calculated several line profiles with the photospheric spectrum properly treated as a lower boundary

TABLE 1

LINE PROFILES FOR $w = 0.01 + 0.99(1 - x^{-1})^{1/2}$, $\tau(w)$ FROM EQUATION (7)

	β = 0.5			α = +2					β = 0.5			α = +1				
v/v_∞	$T=10^3$	10	4	2	1	0.4	0.2	0.1	$T=10^3$	10	4	2	1	0.4	0.2	0.1
-0.95	0.01	0.01	0.01	0.02	0.10	0.38	0.61	0.78	0.01	0.01	0.02	0.05	0.19	0.51	0.71	0.84
-0.90	0.01	0.02	0.02	0.04	0.15	0.45	0.66	0.81	0.01	0.02	0.03	0.08	0.24	0.56	0.74	0.86
-0.80	0.06	0.06	0.07	0.11	0.26	0.56	0.75	0.87	0.06	0.06	0.08	0.14	0.33	0.63	0.79	0.89
-0.70	0.13	0.13	0.15	0.21	0.39	0.67	0.81	0.90	0.13	0.14	0.16	0.23	0.42	0.68	0.82	0.91
-0.60	0.24	0.24	0.26	0.35	0.54	0.76	0.87	0.94	0.24	0.25	0.26	0.34	0.51	0.74	0.86	0.93
-0.50	0.40	0.40	0.42	0.52	0.69	0.86	0.93	0.96	0.40	0.40	0.41	0.48	0.62	0.80	0.89	0.94
-0.40	0.59	0.58	0.61	0.71	0.84	0.94	0.98	0.99	0.59	0.58	0.59	0.63	0.74	0.87	0.93	0.96
-0.30	0.79	0.80	0.84	0.93	1.00	1.03	1.02	1.01	0.79	0.78	0.78	0.81	0.87	0.93	0.97	0.98
-0.20	1.00	1.00	1.09	1.15	1.16	1.11	1.07	1.04	1.00	0.99	1.00	1.00	1.01	1.01	1.01	1.01
-0.10	1.16	1.29	1.37	1.38	1.32	1.19	1.11	1.06	1.16	1.16	1.18	1.20	1.18	1.11	1.06	1.03
-0.05	1.21	1.48	1.52	1.49	1.39	1.23	1.13	1.07	1.21	1.24	1.31	1.33	1.29	1.18	1.10	1.06
-0.01	1.38	1.66	1.64	1.58	1.45	1.25	1.15	1.08	1.22	1.44	1.51	1.50	1.42	1.26	1.15	1.09
0.01	1.72	1.71	1.67	1.60	1.46	1.26	1.15	1.08	1.72	1.71	1.68	1.62	1.50	1.30	1.18	1.10
0.05	1.71	1.70	1.66	1.58	1.45	1.25	1.14	1.08	1.71	1.69	1.67	1.61	1.48	1.28	1.16	1.09
0.10	1.68	1.67	1.63	1.56	1.42	1.24	1.13	1.07	1.68	1.67	1.64	1.58	1.45	1.26	1.15	1.08
0.20	1.59	1.58	1.55	1.49	1.37	1.21	1.12	1.06	1.59	1.57	1.55	1.50	1.38	1.21	1.12	1.06
0.30	1.48	1.47	1.45	1.41	1.32	1.18	1.11	1.06	1.48	1.47	1.45	1.41	1.32	1.18	1.10	1.05
0.40	1.37	1.36	1.35	1.33	1.27	1.16	1.09	1.05	1.37	1.36	1.35	1.32	1.26	1.14	1.08	1.04
0.50	1.26	1.26	1.26	1.25	1.21	1.13	1.08	1.04	1.26	1.26	1.26	1.25	1.20	1.12	1.07	1.04
0.60	1.17	1.17	1.78	1.18	1.16	1.11	1.06	1.04	1.17	1.17	1.18	1.18	1.15	1.09	1.05	1.03
0.70	1.10	1.10	1.11	1.12	1.12	1.08	1.05	1.03	1.10	1.10	1.12	1.12	1.11	1.07	1.04	1.02
0.80	1.04	1.05	1.06	1.07	1.07	1.05	1.03	1.02	1.04	1.05	1.06	1.07	1.07	1.05	1.03	1.02
0.90	1.01	1.02	1.02	1.03	1.03	1.03	1.02	1.01	1.01	1.02	1.03	1.03	1.03	1.02	1.01	1.01
W_R	-0.30	-0.30	-0.29	-0.27	-0.22	-0.13	-0.07	-0.04	-0.30	-0.30	-0.29	-0.27	-0.22	-0.13	-0.07	-0.04
W_B	0.49	0.46	0.43	0.38	0.29	0.16	0.09	0.05	0.49	0.49	0.47	0.43	0.33	0.18	0.10	0.05
W_T	0.19	0.16	0.14	0.11	0.07	0.03	0.02	0.01	0.19	0.19	0.18	0.16	0.11	0.05	0.03	0.10
$-W_R/W_B$	0.61	0.64	0.67	0.71	0.76	0.81	0.82	0.84	0.61	0.60	0.61	0.63	0.66	0.70	0.71	0.73

TABLE 1—*Continued*

v/v_∞	β = 0.5 α = 0								β = 0.5 α = −1							
	$T=10^3$	10	4	2	1	0.4	0.2	0.1	10^3	10^2	10	4	2	1	0.4	0.2
−0.95	0.01	0.01	0.04	0.17	0.41	0.69	0.84	0.92	0.01	0.01	0.14	0.45	0.66	0.82	0.92	0.96
−0.90	0.01	0.03	0.06	0.21	0.44	0.72	0.84	0.92	0.01	0.02	0.16	0.46	0.67	0.82	0.93	0.96
−0.80	0.06	0.07	0.11	0.26	0.49	0.74	0.86	0.93	0.06	0.06	0.19	0.46	0.68	0.82	0.93	0.96
−0.70	0.13	0.14	0.19	0.32	0.53	0.76	0.87	0.93	0.13	0.13	0.23	0.48	0.69	0.81	0.92	0.96
−0.60	0.24	0.25	0.28	0.39	0.56	0.78	0.88	0.94	0.24	0.24	0.29	0.48	0.66	0.80	0.91	0.96
−0.50	0.40	0.40	0.41	0.48	0.61	0.80	0.89	0.94	0.40	0.40	0.40	0.50	0.65	0.79	0.90	0.95
−0.40	0.59	0.58	0.57	0.59	0.68	0.82	0.90	0.94	0.59	0.58	0.55	0.55	0.64	0.76	0.89	0.94
−0.30	0.79	0.77	0.76	0.73	0.75	0.84	0.91	0.95	0.79	0.78	0.73	0.65	0.65	0.74	0.86	0.92
−0.20	1.00	0.97	0.95	0.89	0.85	0.87	0.92	0.95	1.00	0.99	0.92	0.80	0.71	0.71	0.82	0.89
−0.10	1.16	1.13	1.10	1.04	0.96	0.91	0.93	0.96	1.16	1.15	1.07	0.95	0.83	0.73	0.73	0.81
−0.05	1.21	1.18	1.15	1.09	1.01	0.95	0.95	0.96	1.21	1.19	1.12	1.00	0.88	0.76	0.68	0.71
−0.01	1.22	1.20	1.16	1.11	1.03	0.98	0.97	0.97	1.22	1.21	1.14	1.01	0.89	0.78	0.67	0.62
0.01	1.72	1.70	1.66	1.59	1.46	1.29	1.19	1.11	1.72	1.71	1.64	1.51	1.39	1.28	1.17	1.12
0.05	1.71	1.68	1.65	1.58	1.45	1.27	1.16	1.09	1.71	1.70	1.63	1.50	1.38	1.27	1.15	1.09
0.10	1.68	1.65	1.62	1.55	1.42	1.23	1.14	1.07	1.68	1.67	1.60	1.47	1.35	1.23	1.12	1.07
0.20	1.59	1.56	1.53	1.46	1.34	1.18	1.10	1.05	1.59	1.58	1.51	1.39	1.27	1.16	1.07	1.04
0.30	1.48	1.46	1.44	1.37	1.27	1.14	1.07	1.04	1.48	1.47	1.41	1.30	1.19	1.11	1.05	1.03
0.40	1.37	1.36	1.34	1.29	1.21	1.11	1.06	1.03	1.37	1.36	1.32	1.23	1.14	1.08	1.04	1.02
0.50	1.26	1.26	1.25	1.22	1.16	1.08	1.04	1.02	1.26	1.26	1.24	1.17	1.10	1.06	1.03	1.01
0.60	1.17	1.18	1.18	1.16	1.12	1.06	1.03	1.02	1.17	1.17	1.17	1.12	1.08	1.04	1.02	1.01
0.70	1.10	1.11	1.12	1.11	1.08	1.04	1.02	1.01	1.10	1.10	1.12	1.08	1.05	1.03	1.01	1.01
0.80	1.04	1.06	1.07	1.07	1.05	1.03	1.02	1.01	1.05	1.05	1.07	1.05	1.03	1.02	1.01	1.00
0.90	1.01	1.02	1.03	1.03	1.03	1.02	1.01	1.00	1.01	1.02	1.03	1.03	1.02	1.01	1.00	1.00
W_R	−0.30	−0.30	−0.29	−0.25	−0.19	−0.10	−0.06	−0.03	−0.30	−0.30	−0.27	−0.20	−0.14	−0.09	−0.04	−0.02
W_B	0.49	0.50	0.49	0.44	0.34	0.19	0.11	0.06	0.49	0.50	0.48	0.39	0.30	0.22	0.13	0.08
W_T	0.19	0.20	0.20	0.19	0.15	0.09	0.05	0.03	0.19	0.20	0.20	0.19	0.16	0.13	0.09	0.06
$-W_R/W_B$	0.61	0.59	0.58	0.57	0.55	0.53	0.52	0.52	0.61	0.60	0.57	0.52	0.46	0.39	0.32	0.28

TABLE 1—*Continued*

	$\beta = 0.5$			$\alpha = -2$					$\beta = 0.5$			$\alpha = -3$				
v/v_∞	$T=10^3$	2.10^2	10^2	40	10	4	2	1	10^5	2.10^4	10^4	4.10^3	2.10^3	10^3	10^2	10
-0.95	0.01	0.14	0.37	0.67	0.91	0.97	0.99	0.99	0.01	0.03	0.13	0.44	0.66	0.81	0.98	1.00
-0.90	0.03	0.15	0.37	0.67	0.90	0.96	0.98	0.99	0.02	0.04	0.13	0.42	0.64	0.80	0.98	1.00
-0.80	0.07	0.16	0.35	0.64	0.89	0.96	0.98	0.99	0.06	0.08	0.13	0.36	0.58	0.76	0.97	1.00
-0.70	0.14	0.20	0.33	0.60	0.88	0.95	0.97	0.99	0.13	0.15	0.17	0.30	0.50	0.70	0.96	1.00
-0.60	0.25	0.27	0.33	0.56	0.85	0.94	0.97	0.98	0.24	0.25	0.26	0.29	0.43	0.61	0.95	1.00
-0.50	0.40	0.39	0.38	0.51	0.81	0.91	0.96	0.98	0.40	0.40	0.39	0.35	0.38	0.52	0.92	0.99
-0.40	0.58	0.55	0.51	0.50	0.74	0.88	0.94	0.97	0.58	0.57	0.56	0.50	0.44	0.46	0.86	0.99
-0.30	0.78	0.74	0.68	0.58	0.66	0.81	0.90	0.95	0.78	0.77	0.75	0.68	0.60	0.53	0.75	0.97
-0.20	0.98	0.93	0.87	0.74	0.60	0.70	0.81	0.89	0.99	0.97	0.94	0.87	0.79	0.70	0.58	0.91
-0.10	1.14	1.09	1.02	0.89	0.69	0.60	0.61	0.70	1.15	1.12	1.10	1.02	0.94	0.85	0.60	0.64
-0.05	1.18	1.13	1.07	0.94	0.75	0.65	0.60	0.56	1.19	1.17	1.15	1.07	0.99	0.90	0.66	0.54
-0.01	1.20	1.15	1.08	0.95	0.76	0.68	0.63	0.59	1.21	1.19	1.16	1.09	1.00	0.91	0.68	0.57
0.01	1.70	1.65	1.58	1.45	1.26	1.18	1.13	1.09	1.71	1.69	1.66	1.59	1.50	1.41	1.18	1.07
0.05	1.69	1.64	1.57	1.44	1.25	1.16	1.11	1.07	1.70	1.67	1.65	1.58	1.49	1.40	1.17	1.05
0.10	1.66	1.61	1.54	1.41	1.21	1.12	1.07	1.04	1.67	1.64	1.62	1.55	1.46	1.37	1.13	1.02
0.20	1.57	1.52	1.46	1.33	1.14	1.06	1.03	1.02	1.58	1.56	1.53	1.46	1.38	1.29	1.06	1.01
0.30	1.46	1.42	1.36	1.24	1.08	1.04	1.02	1.01	1.47	1.45	1.43	1.37	1.29	1.20	1.03	1.00
0.40	1.36	1.33	1.27	1.17	1.06	1.02	1.01	1.01	1.36	1.35	1.34	1.28	1.20	1.13	1.02	1.00
0.50	1.26	1.24	1.20	1.12	1.04	1.02	1.01	1.00	1.26	1.26	1.25	1.20	1.14	1.08	1.01	1.00
0.60	1.18	1.17	1.14	1.08	1.03	1.01	1.01	1.00	1.17	1.18	1.18	1.14	1.09	1.06	1.01	1.00
0.70	1.11	1.12	1.10	1.05	1.02	1.01	1.00	1.00	1.10	1.12	1.12	1.09	1.06	1.04	1.00	1.00
0.80	1.06	1.07	1.06	1.03	1.01	1.00	1.00	1.00	1.05	1.07	1.07	1.05	1.04	1.02	1.00	1.00
0.90	1.02	1.03	1.03	1.02	1.01	1.00	1.00	1.00	1.02	1.03	1.03	1.03	1.02	1.01	1.00	1.00
W_R	-0.29	-0.28	-0.24	-0.16	-0.07	-0.04	-0.02	-0.01	-0.30	-0.29	-0.28	-0.24	-0.19	-0.14	-0.03	-0.01
W_B	0.50	0.48	0.44	0.35	0.21	0.14	0.11	0.08	0.50	0.50	0.49	0.44	0.38	0.32	0.16	0.07
W_T	0.20	0.20	0.20	0.18	0.14	0.11	0.08	0.06	0.20	0.20	0.20	0.20	0.20	0.18	0.12	0.06
$-W_R/W_B$	0.59	0.58	0.55	0.47	0.33	0.24	0.19	0.15	0.60	0.59	0.58	0.54	0.49	0.43	0.21	0.09

TABLE 2

LINE PROFILES FOR $w = 0.01 + 0.99(1 - x^{-1})$, $\tau(w)$ FROM EQUATION (7)

	$\beta = 1$			$\alpha = +2$					$\beta = 1$			$\alpha = +1$				
v/v_∞	$T=10^3$	10	4	2	1	0.4	0.2	0.1	10^3	10	4	2	1	0.4	0.2	0.1
-0.95	0.01	0.01	0.02	0.02	0.09	0.36	0.59	0.77	0.01	0.01	0.02	0.04	0.18	0.49	0.69	0.84
-0.90	0.02	0.02	0.03	0.04	0.13	0.42	0.64	0.81	0.02	0.02	0.03	0.07	0.21	0.53	0.72	0.85
-0.80	0.05	0.06	0.07	0.11	0.24	0.54	0.73	0.86	0.05	0.06	0.07	0.13	0.30	0.59	0.77	0.88
-0.70	0.12	0.12	0.13	0.20	0.38	0.66	0.81	0.90	0.12	0.12	0.14	0.21	0.39	0.67	0.81	0.90
-0.60	0.21	0.21	0.24	0.33	0.53	0.77	0.88	0.94	0.21	0.21	0.23	0.32	0.49	0.74	0.86	0.93
-0.50	0.34	0.34	0.38	0.51	0.71	0.88	0.94	0.97	0.34	0.34	0.36	0.45	0.62	0.81	0.90	0.95
-0.40	0.52	0.52	0.59	0.74	0.89	0.98	1.00	1.00	0.52	0.52	0.53	0.62	0.76	0.89	0.95	0.97
-0.30	0.73	0.74	0.86	1.00	1.07	1.07	1.05	1.03	0.73	0.73	0.74	0.82	0.91	0.97	0.99	1.00
-0.20	0.99	1.05	1.19	1.26	1.24	1.15	1.09	1.05	0.99	0.98	1.00	1.05	1.08	1.07	1.04	1.02
-0.10	1.27	1.48	1.54	1.49	1.38	1.21	1.12	1.06	1.27	1.27	1.31	1.34	1.29	1.17	1.10	1.05
-0.05	1.41	1.71	1.69	1.58	1.43	1.23	1.13	1.07	1.41	1.44	1.50	1.51	1.41	1.24	1.13	1.07
-0.01	1.65	1.89	1.79	1.64	1.46	1.25	1.14	1.07	1.50	1.70	1.75	1.70	1.55	1.31	1.18	1.09
0.01	2.01	1.92	1.80	1.64	1.46	1.25	1.14	1.07	2.01	1.98	1.92	1.81	1.62	1.34	1.19	1.10
0.05	1.97	1.90	1.78	1.63	1.45	1.24	1.14	1.07	1.97	1.94	1.89	1.77	1.58	1.31	1.17	1.09
0.10	1.89	1.85	1.75	1.61	1.44	1.24	1.13	1.07	1.89	1.87	1.83	1.72	1.53	1.28	1.16	1.08
0.20	1.73	1.73	1.65	1.54	1.40	1.22	1.12	1.07	1.73	1.71	1.68	1.60	1.44	1.24	1.13	1.07
0.30	1.57	1.56	1.53	1.46	1.35	1.20	1.11	1.06	1.57	1.56	1.53	1.48	1.37	1.20	1.11	1.06
0.40	1.42	1.41	1.40	1.37	1.30	1.17	1.10	1.06	1.42	1.41	1.40	1.37	1.29	1.17	1.09	1.05
0.50	1.29	1.29	1.29	1.28	1.24	1.15	1.09	1.05	1.29	1.29	1.29	1.28	1.23	1.13	1.08	1.04
0.60	1.19	1.19	1.19	1.20	1.18	1.12	1.07	1.04	1.19	1.19	1.20	1.20	1.17	1.10	1.06	1.03
0.70	1.10	1.11	1.12	1.13	1.13	1.09	1.06	1.03	1.10	1.11	1.12	1.13	1.12	1.08	1.05	1.03
0.80	1.05	1.05	1.06	1.07	1.08	1.06	1.04	1.02	1.05	1.05	1.07	1.08	1.07	1.05	1.03	1.02
0.90	1.01	1.02	1.02	1.03	1.03	1.03	1.02	1.01	1.01	1.02	1.03	1.03	1.03	1.02	1.02	1.01
W_R	-0.36	-0.36	-0.33	-0.29	-0.23	-0.14	-0.08	-0.04	-0.36	-0.36	-0.35	-0.32	-0.25	-0.14	-0.08	-0.04
W_B	0.50	0.45	0.41	0.35	0.26	0.15	0.09	0.05	0.50	0.49	0.47	0.41	0.31	0.17	0.09	0.05
W_T	0.13	0.10	0.08	0.05	0.03	0.01	0.01	0.00	0.13	0.13	0.12	0.09	0.06	0.03	0.01	0.01
$-W_R/W_B$	0.74	0.78	0.82	0.85	0.88	0.91	0.92	0.94	0.73	0.73	0.74	0.78	0.81	0.85	0.86	0.88

TABLE 2—*Continued*

	$\beta = 1$		$\alpha = 0$						$\beta = 1$		$\alpha = -1$					
v/v_∞	$T=10^3$	10	4	2	1	0.4	0.2	0.1	10^3	10^2	10	4	2	1	0.4	0.2
-0.95	0.01	0.02	0.04	0.16	0.39	0.68	0.83	0.91	0.01	0.01	0.13	0.42	0.65	0.81	0.92	0.96
-0.90	0.02	0.03	0.06	0.18	0.41	0.69	0.83	0.91	0.02	0.02	0.14	0.42	0.65	0.80	0.92	0.96
-0.80	0.05	0.07	0.10	0.23	0.45	0.72	0.84	0.92	0.05	0.06	0.16	0.42	0.64	0.80	0.91	0.95
-0.70	0.12	0.13	0.16	0.29	0.49	0.75	0.86	0.93	0.12	0.12	0.20	0.43	0.64	0.79	0.91	0.95
-0.60	0.21	0.21	0.25	0.36	0.54	0.77	0.87	0.93	0.21	0.21	0.26	0.43	0.63	0.78	0.90	0.95
-0.50	0.34	0.34	0.36	0.44	0.59	0.79	0.89	0.94	0.34	0.34	0.35	0.45	0.62	0.77	0.89	0.94
-0.40	0.52	0.51	0.51	0.56	0.66	0.82	0.90	0.95	0.52	0.52	0.48	0.50	0.61	0.74	0.88	0.94
-0.30	0.73	0.71	0.70	0.70	0.75	0.86	0.92	0.96	0.73	0.72	0.67	0.59	0.62	0.72	0.85	0.92
-0.20	0.99	0.96	0.94	0.90	0.87	0.91	0.94	0.97	0.99	0.98	0.91	0.79	0.69	0.71	0.82	0.89
-0.10	1.27	1.25	1.21	1.14	1.04	0.98	0.98	0.99	1.27	1.26	1.19	1.06	0.91	0.77	0.75	0.82
-0.05	1.41	1.38	1.35	1.27	1.14	1.04	1.01	1.00	1.41	1.40	1.33	1.20	1.05	0.89	0.75	0.75
-0.01	1.50	1.47	1.44	1.36	1.23	1.10	1.06	1.03	1.50	1.49	1.42	1.29	1.14	0.99	0.82	0.73
0.01	2.01	1.98	1.94	1.85	1.67	1.42	1.27	1.16	2.00	1.99	1.92	1.79	1.64	1.50	1.33	1.23
0.05	1.97	1.93	1.90	1.81	1.63	1.37	1.21	1.12	1.96	1.95	1.88	1.75	1.60	1.45	1.27	1.16
0.10	1.89	1.87	1.83	1.74	1.56	1.30	1.17	1.09	1.89	1.88	1.81	1.68	1.53	1.36	1.19	1.10
0.20	1.73	1.70	1.67	1.59	1.43	1.22	1.12	1.06	1.73	1.72	1.66	1.53	1.37	1.23	1.11	1.06
0.30	1.57	1.55	1.53	1.45	1.33	1.17	1.09	1.05	1.57	1.56	1.51	1.39	1.26	1.15	1.07	1.04
0.40	1.42	1.41	1.40	1.34	1.25	1.13	1.07	1.04	1.42	1.41	1.38	1.28	1.18	1.11	1.05	1.02
0.50	1.29	1.29	1.29	1.26	1.19	1.10	1.05	1.03	1.29	1.29	1.27	1.20	1.13	1.08	1.03	1.02
0.60	1.19	1.19	1.20	1.18	1.14	1.07	1.04	1.02	1.19	1.19	1.19	1.14	1.09	1.05	1.02	1.01
0.70	1.10	1.12	1.13	1.12	1.10	1.05	1.03	1.02	1.10	1.11	1.13	1.10	1.06	1.04	1.02	1.01
0.80	1.05	1.06	1.07	1.08	1.06	1.03	1.02	1.01	1.05	1.05	1.08	1.06	1.04	1.02	1.01	1.01
0.90	1.01	1.02	1.03	1.03	1.03	1.02	1.01	1.01	1.01	1.02	1.03	1.03	1.02	1.01	1.00	1.00
W_R	-0.36	-0.36	-0.35	-0.31	-0.23	-0.13	-0.07	-0.04	-0.36	-0.36	-0.34	-0.27	-0.19	-0.13	-0.06	-0.04
W_B	0.50	0.50	0.49	0.44	0.34	0.18	0.10	0.06	0.50	0.50	0.49	0.40	0.31	0.22	0.13	0.08
W_T	0.13	0.14	0.14	0.13	0.10	0.06	0.03	0.02	0.13	0.14	0.14	0.13	0.12	0.10	0.07	0.05
$-W_R/W_B$	0.73	0.72	0.71	0.70	0.70	0.69	0.70	0.69	0.73	0.72	0.71	0.67	0.63	0.56	0.49	0.44

TABLE 2—*Continued*

	$\beta = 1$		$\alpha = -2$						$\beta = 1$		$\alpha = -3$					
v/v_∞	$T=10^3$	2.10^2	10^2	4.10^1	10	4	2	1	10^5	2.10^4	10^4	4.10^3	2.10^3	10^3	10^2	10
-0.95	0.02	0.13	0.35	0.65	0.90	0.96	0.98	0.99	0.01	0.03	0.12	0.42	0.64	0.80	0.98	1.00
-0.90	0.03	0.13	0.33	0.64	0.89	0.96	0.98	0.99	0.02	0.04	0.11	0.38	0.61	0.79	0.98	1.00
-0.80	0.06	0.13	0.30	0.60	0.88	0.95	0.97	0.99	0.06	0.07	0.11	0.30	0.54	0.73	0.97	1.00
-0.70	0.13	0.16	0.27	0.55	0.86	0.94	0.97	0.98	0.12	0.14	0.14	0.25	0.44	0.65	0.96	1.00
-0.60	0.21	0.23	0.28	0.50	0.82	0.92	0.96	0.98	0.21	0.22	0.22	0.24	0.35	0.55	0.94	0.99
-0.50	0.34	0.33	0.32	0.44	0.77	0.90	0.95	0.97	0.34	0.34	0.33	0.30	0.30	0.43	0.90	0.99
-0.40	0.51	0.49	0.44	0.43	0.70	0.86	0.92	0.96	0.52	0.51	0.50	0.45	0.38	0.36	0.83	0.98
-0.30	0.71	0.68	0.63	0.51	0.60	0.78	0.88	0.93	0.72	0.70	0.69	0.63	0.55	0.47	0.68	0.96
-0.20	0.97	0.93	0.87	0.73	0.55	0.65	0.77	0.87	0.98	0.96	0.94	0.87	0.79	0.70	0.49	0.88
-0.10	1.25	1.21	1.14	1.01	0.76	0.62	0.60	0.67	1.26	1.24	1.22	1.15	1.07	0.97	0.66	0.57
-0.05	1.39	1.34	1.28	1.15	0.91	0.77	0.68	0.61	1.40	1.38	1.35	1.29	1.21	1.11	0.81	0.60
-0.01	1.48	1.43	1.37	1.24	1.00	0.87	0.79	0.73	1.49	1.47	1.44	1.38	1.29	1.20	0.90	0.72
0.01	1.98	1.94	1.87	1.74	1.50	1.37	1.29	1.23	1.99	1.97	1.95	1.88	1.80	1.70	1.41	1.22
0.05	1.94	1.90	1.83	1.70	1.46	1.33	1.24	1.16	1.95	1.93	1.91	1.84	1.76	1.66	1.36	1.15
0.10	1.87	1.83	1.76	1.63	1.38	1.23	1.14	1.08	1.88	1.86	1.84	1.77	1.69	1.59	1.28	1.06
0.20	1.71	1.67	1.61	1.48	1.22	1.11	1.06	1.03	1.72	1.70	1.68	1.61	1.54	1.44	1.12	1.02
0.30	1.55	1.52	1.46	1.33	1.13	1.06	1.03	1.02	1.56	1.54	1.53	1.47	1.39	1.30	1.06	1.01
0.40	1.41	1.39	1.34	1.23	1.08	1.04	1.02	1.01	1.41	1.40	1.39	1.34	1.27	1.19	1.03	1.00
0.50	1.29	1.28	1.24	1.15	1.05	1.02	1.01	1.01	1.29	1.29	1.28	1.24	1.18	1.12	1.02	1.00
0.60	1.19	1.19	1.17	1.10	1.03	1.01	1.01	1.01	1.19	1.19	1.19	1.16	1.12	1.07	1.01	1.00
0.70	1.11	1.13	1.11	1.07	1.02	1.01	1.00	1.00	1.11	1.12	1.13	1.10	1.07	1.04	1.01	1.00
0.80	1.06	1.08	1.06	1.04	1.01	1.01	1.00	1.00	1.05	1.07	1.07	1.06	1.04	1.02	1.00	1.00
0.90	1.02	1.03	1.03	1.02	1.01	1.00	1.00	1.00	1.02	1.03	1.03	1.03	1.02	1.01	1.00	1.00
W_R	-0.36	-0.35	-0.31	-0.23	-0.11	-0.06	-0.04	-0.02	-0.36	-0.36	-0.35	-0.31	-0.26	-0.21	-0.07	-0.02
W_B	0.50	0.49	0.45	0.36	0.22	0.15	0.11	0.08	0.50	0.50	0.49	0.45	0.40	0.34	0.17	0.07
W_T	0.14	0.14	0.14	0.13	0.11	0.09	0.07	0.06	0.14	0.14	0.14	0.14	0.14	0.13	0.10	0.06
$-W_R/W_B$	0.72	0.71	0.69	0.64	0.52	0.43	0.36	0.31	0.72	0.72	0.71	0.69	0.66	0.62	0.41	0.24

TABLE 3

LINE PROFILES FOR $w = 0.01 + 0.99(1 - x^{-1})^{1/2}$, $\tau(w)$ FROM EQUATION (8)

	$\beta = 0.5$			$\gamma = 0.5$					$\beta = 0.5$			$\gamma = 1$				
v/v_∞	$T=10^3$	10	4	2	1	0.5	0.25	0.1	10^3	10	4	2	1	0.5	0.25	0.1
-0.95	0.01	0.07	0.31	0.55	0.74	0.86	0.93	0.98	0.01	0.42	0.71	0.84	0.92	0.96	0.98	0.99
-0.90	0.01	0.05	0.23	0.46	0.68	0.82	0.91	0.96	0.02	0.21	0.53	0.73	0.85	0.93	0.96	0.99
-0.80	0.06	0.09	0.19	0.40	0.62	0.78	0.88	0.95	0.06	0.18	0.34	0.58	0.76	0.87	0.93	0.97
-0.70	0.13	0.14	0.22	0.37	0.58	0.76	0.87	0.95	0.13	0.15	0.28	0.48	0.68	0.82	0.91	0.96
-0.60	0.24	0.25	0.27	0.38	0.58	0.74	0.86	0.94	0.24	0.24	0.27	0.42	0.62	0.78	0.88	0.95
-0.50	0.39	0.39	0.38	0.44	0.58	0.74	0.85	0.93	0.39	0.36	0.35	0.42	0.58	0.74	0.86	0.94
-0.40	0.58	0.56	0.53	0.53	0.61	0.74	0.84	0.93	0.58	0.53	0.49	0.48	0.58	0.72	0.84	0.93
-0.30	0.79	0.76	0.71	0.66	0.67	0.75	0.84	0.93	0.79	0.73	0.66	0.60	0.62	0.71	0.82	0.92
-0.20	0.99	0.96	0.91	0.83	0.77	0.78	0.84	0.92	0.99	0.92	0.85	0.77	0.71	0.73	0.81	0.90
-0.10	1.16	1.12	1.06	0.98	0.89	0.84	0.86	0.92	1.15	1.08	1.01	0.92	0.83	0.79	0.81	0.89
-0.05	1.21	1.17	1.11	1.03	0.94	0.88	0.88	0.92	1.20	1.13	1.06	0.97	0.88	0.83	0.83	0.89
-0.01	1.23	1.18	1.13	1.05	0.96	0.91	0.91	0.94	1.22	1.15	1.07	0.99	0.90	0.85	0.86	0.90
0.01	1.73	1.68	1.63	1.54	1.42	1.30	1.21	1.12	1.72	1.65	1.57	1.49	1.39	1.28	1.20	1.12
0.05	1.71	1.67	1.62	1.53	1.41	1.29	1.19	1.09	1.71	1.63	1.56	1.47	1.37	1.26	1.18	1.09
0.10	1.68	1.64	1.59	1.50	1.38	1.25	1.15	1.07	1.68	1.60	1.53	1.44	1.33	1.23	1.14	1.07
0.20	1.59	1.55	1.50	1.41	1.30	1.18	1.10	1.05	1.58	1.51	1.44	1.36	1.25	1.16	1.09	1.04
0.30	1.48	1.45	1.40	1.32	1.22	1.13	1.07	1.03	1.47	1.41	1.35	1.27	1.18	1.10	1.06	1.02
0.40	1.36	1.34	1.31	1.24	1.16	1.09	1.05	1.02	1.36	1.32	1.26	1.19	1.12	1.07	1.04	1.02
0.50	1.26	1.25	1.23	1.18	1.11	1.07	1.04	1.02	1.26	1.23	1.18	1.13	1.08	1.04	1.02	1.01
0.60	1.17	1.18	1.16	1.12	1.08	1.05	1.03	1.01	1.17	1.16	1.12	1.08	1.05	1.03	1.01	1.01
0.70	1.10	1.11	1.10	1.08	1.05	1.03	1.02	1.01	1.10	1.10	1.07	1.05	1.03	1.02	1.01	1.00
0.80	1.04	1.07	1.06	1.05	1.03	1.02	1.01	1.00	1.05	1.06	1.04	1.02	1.01	1.01	1.00	1.00
0.90	1.01	1.03	1.03	1.02	1.01	1.01	1.00	1.00	1.01	1.02	1.01	1.01	1.00	1.00	1.00	1.00
W_R	-0.30	-0.30	-0.27	-0.22	-0.15	-0.10	-0.06	-0.03	-0.30	-0.27	-0.23	-0.18	-0.12	-0.08	-0.05	-0.02
W_B	0.50	0.50	0.47	0.41	0.31	0.21	0.13	0.06	0.49	0.47	0.42	0.36	0.29	0.20	0.13	0.06
W_T	0.19	0.20	0.20	0.19	0.16	0.12	0.07	0.03	0.19	0.20	0.20	0.19	0.16	0.12	0.08	0.04
$-W_R/W_B$	0.61	0.60	0.58	0.54	0.49	0.46	0.44	0.43	0.61	0.58	0.54	0.49	0.44	0.39	0.37	0.36

TABLE 3—*Continued*

v/v_∞	β = 0.5 γ = 2 T=10^3	10^2	10	4	2	1	0.5	0.25	β = 0.5 γ = 4 10^6	10^3	10^2	10	4	2	1	0.5
-0.95	0.01	0.53	0.94	0.98	0.99	0.99	1.00	1.00	0.01	0.98	1.00	1.00	1.00	1.00	1.00	1.00
-0.90	0.02	0.12	0.80	0.92	0.96	0.98	0.99	0.99	0.02	0.72	0.97	1.00	1.00	1.00	1.00	1.00
-0.80	0.06	0.06	0.47	0.73	0.86	0.92	0.96	0.98	0.06	0.06	0.65	0.96	0.98	0.99	1.00	1.00
-0.70	0.13	0.12	0.25	0.54	0.73	0.85	0.92	0.96	0.13	0.10	0.21	0.82	0.92	0.96	0.98	0.99
-0.60	0.24	0.22	0.22	0.39	0.59	0.76	0.87	0.93	0.24	0.19	0.16	0.57	0.79	0.89	0.94	0.97
-0.50	0.39	0.36	0.30	0.34	0.49	0.67	0.81	0.90	0.39	0.33	0.27	0.35	0.59	0.75	0.86	0.93
-0.40	0.57	0.54	0.45	0.41	0.45	0.59	0.74	0.86	0.58	0.50	0.43	0.34	0.43	0.59	0.74	0.86
-0.30	0.77	0.74	0.64	0.56	0.52	0.57	0.69	0.81	0.79	0.70	0.62	0.49	0.44	0.49	0.61	0.75
-0.20	0.97	0.94	0.83	0.75	0.68	0.63	0.66	0.76	0.99	0.89	0.81	0.68	0.61	0.56	0.55	0.64
-0.10	1.14	1.10	0.98	0.90	0.83	0.75	0.71	0.74	1.16	1.05	0.97	0.83	0.76	0.71	0.65	0.62
-0.05	1.19	1.15	1.03	0.95	0.87	0.80	0.75	0.76	1.21	1.10	1.02	0.88	0.81	0.76	0.71	0.67
-0.01	1.20	1.16	1.05	0.97	0.89	0.82	0.77	0.78	1.23	1.12	1.04	0.90	0.83	0.78	0.73	0.69
0.01	1.70	1.66	1.55	1.47	1.39	1.31	1.23	1.17	1.73	1.62	1.54	1.40	1.33	1.28	1.23	1.18
0.05	1.69	1.65	1.54	1.46	1.38	1.30	1.22	1.15	1.71	1.61	1.52	1.39	1.32	1.26	1.21	1.16
0.10	1.66	1.62	1.51	1.43	1.35	1.26	1.18	1.12	1.68	1.58	1.49	1.36	1.29	1.23	1.17	1.08
0.20	1.57	1.53	1.42	1.34	1.26	1.18	1.11	1.06	1.59	1.48	1.41	1.27	1.20	1.14	1.09	1.03
0.30	1.46	1.42	1.33	1.25	1.18	1.11	1.06	1.03	1.48	1.38	1.31	1.18	1.11	1.07	1.04	1.01
0.40	1.35	1.32	1.23	1.16	1.11	1.06	1.03	1.02	1.36	1.28	1.22	1.10	1.05	1.03	1.02	1.01
0.50	1.25	1.23	1.16	1.10	1.06	1.03	1.02	1.01	1.26	1.19	1.14	1.04	1.02	1.01	1.01	1.00
0.60	1.17	1.15	1.09	1.05	1.03	1.02	1.01	1.01	1.17	1.12	1.07	1.02	1.01	1.00	1.00	1.00
0.70	1.10	1.09	1.05	1.03	1.01	1.01	1.00	1.00	1.10	1.07	1.03	1.00	1.00	1.00	1.00	1.00
0.80	1.05	1.05	1.02	1.01	1.01	1.00	1.00	1.00	1.04	1.03	1.01	1.00	1.00	1.00	1.00	1.00
0.90	1.02	1.02	1.00	1.00	1.00	1.00	1.00	1.00	1.01	1.00	1.00	1.00	1.00	1.00	1.00	1.00
W_R	-0.30	-0.28	-0.21	-0.16	-0.12	-0.08	-0.05	-0.03	-0.30	-0.24	-0.19	-0.12	-0.08	-0.06	-0.04	-0.03
W_B	0.49	0.47	0.40	0.35	0.30	0.24	0.18	0.12	0.50	0.44	0.39	0.30	0.26	0.22	0.18	0.14
W_T	0.20	0.20	0.20	0.19	0.18	0.16	0.12	0.09	0.19	0.20	0.20	0.18	0.17	0.16	0.14	0.11
$-W_R/W_B$	0.60	0.58	0.51	0.46	0.40	0.35	0.30	0.28	0.61	0.55	0.50	0.39	0.33	0.28	0.24	0.20

TABLE 4

LINE PROFILES FOR $w = 0.01 + 0.99(1 - x^{-1})$, $\tau(w)$ FROM EQUATION (8)

	β = 1	γ = 0.5							β = 1	γ = 1						
v/v_∞	$T=10^3$	10	4	2	1	0.5	0.25	0.1	10^3	10	4	2	1	0.5	0.25	0.1
-0.95	0.01	0.06	0.29	0.53	0.73	0.85	0.93	0.97	0.01	0.39	0.68	0.83	0.91	0.96	0.98	1.00
-0.90	0.01	0.04	0.19	0.42	0.65	0.80	0.90	0.96	0.02	0.18	0.49	0.69	0.83	0.92	0.96	0.99
-0.80	0.05	0.07	0.15	0.35	0.58	0.75	0.87	0.94	0.05	0.09	0.28	0.51	0.71	0.84	0.92	0.96
-0.70	0.11	0.13	0.18	0.33	0.55	0.73	0.85	0.94	0.12	0.12	0.22	0.42	0.63	0.79	0.89	0.95
-0.60	0.21	0.21	0.23	0.34	0.53	0.71	0.84	0.93	0.21	0.20	0.23	0.37	0.57	0.74	0.86	0.94
-0.50	0.34	0.34	0.34	0.40	0.55	0.71	0.84	0.93	0.34	0.32	0.31	0.37	0.54	0.72	0.84	0.93
-0.40	0.52	0.50	0.47	0.48	0.58	0.73	0.84	0.93	0.52	0.48	0.43	0.43	0.54	0.70	0.82	0.92
-0.30	0.73	0.70	0.66	0.63	0.66	0.75	0.85	0.93	0.73	0.67	0.62	0.56	0.60	0.70	0.82	0.92
-0.20	0.98	0.95	0.90	0.83	0.78	0.81	0.87	0.94	0.98	0.92	0.85	0.77	0.71	0.75	0.83	0.92
-0.10	1.27	1.23	1.18	1.09	0.97	0.92	0.92	0.96	1.26	1.20	1.13	1.03	0.92	0.86	0.87	0.93
-0.05	1.41	1.37	1.32	1.23	1.09	0.99	0.97	0.97	1.41	1.34	1.27	1.17	1.05	0.95	0.92	0.95
-0.01	1.51	1.47	1.42	1.33	1.20	1.09	1.04	1.02	1.51	1.44	1.37	1.28	1.15	1.05	1.00	0.99
0.01	2.01	1.97	1.92	1.83	1.67	1.49	1.35	1.21	2.01	1.94	1.87	1.78	1.64	1.48	1.35	1.21
0.05	1.97	1.93	1.88	1.78	1.62	1.44	1.27	1.13	1.96	1.89	1.83	1.73	1.59	1.43	1.28	1.14
0.10	1.89	1.85	1.80	1.71	1.54	1.36	1.21	1.10	1.89	1.82	1.75	1.66	1.51	1.35	1.21	1.10
0.20	1.73	1.69	1.65	1.55	1.40	1.25	1.14	1.06	1.72	1.66	1.60	1.50	1.36	1.23	1.13	1.06
0.30	1.56	1.54	1.50	1.41	1.29	1.18	1.10	1.04	1.56	1.51	1.45	1.36	1.25	1.15	1.08	1.04
0.40	1.41	1.40	1.37	1.30	1.21	1.12	1.07	1.03	1.41	1.37	1.32	1.25	1.17	1.10	1.05	1.02
0.50	1.29	1.28	1.26	1.21	1.15	1.09	1.05	1.02	1.29	1.26	1.22	1.17	1.11	1.06	1.03	1.01
0.60	1.18	1.19	1.18	1.14	1.10	1.06	1.03	1.01	1.18	1.17	1.15	1.11	1.07	1.04	1.02	1.01
0.70	1.10	1.12	1.12	1.09	1.06	1.04	1.02	1.01	1.10	1.11	1.09	1.06	1.04	1.02	1.01	1.00
0.80	1.04	1.07	1.07	1.05	1.03	1.02	1.01	1.00	1.05	1.06	1.04	1.03	1.02	1.01	1.01	1.00
0.90	1.01	1.03	1.03	1.02	1.01	1.01	1.00	1.00	1.01	1.02	1.01	1.01	1.00	1.00	1.00	1.00
W_R	-0.37	-0.36	-0.34	-0.29	-0.21	-0.14	-0.08	-0.04	-0.37	-0.34	-0.31	-0.25	-0.18	-0.12	-0.07	-0.03
W_B	0.49	0.49	0.47	0.41	0.31	0.21	0.12	0.06	0.49	0.47	0.43	0.37	0.29	0.20	0.12	0.06
W_T	0.12	0.13	0.13	0.12	0.10	0.07	0.04	0.02	0.12	0.13	0.13	0.12	0.11	0.08	0.05	0.02
$-W_R/W_B$	0.76	0.74	0.73	0.70	0.67	0.65	0.65	0.65	0.76	0.73	0.71	0.67	0.63	0.60	0.59	0.59

TABLE 4—*Continued*

	$\beta = 1$		$\gamma = 2$						$\beta = 1$		$\gamma = 4$					
v/v_∞	$T=10^3$	10^2	10	4	2	1	0.5	0.25	10^6	10^3	10^2	10	4	2	1	0.5
-0.95	0.02	0.50	0.94	0.98	0.99	1.00	1.00	1.00	0.01	0.98	1.00	1.00	1.00	1.00	1.00	1.00
-0.90	0.02	0.08	0.76	0.90	0.95	0.98	0.99	1.00	0.02	0.65	0.96	1.00	1.00	1.00	1.00	1.00
-0.80	0.06	0.06	0.38	0.67	0.82	0.91	0.95	0.97	0.05	0.04	0.54	0.94	0.97	0.99	0.99	1.00
-0.70	0.12	0.11	0.18	0.44	0.66	0.81	0.90	0.95	0.12	0.09	0.11	0.75	0.89	0.94	0.97	0.99
-0.60	0.21	0.19	0.16	0.30	0.51	0.70	0.84	0.91	0.21	0.16	0.12	0.43	0.70	0.84	0.91	0.96
-0.50	0.33	0.31	0.25	0.27	0.41	0.60	0.77	0.88	0.34	0.28	0.23	0.23	0.46	0.67	0.81	0.90
-0.40	0.51	0.48	0.41	0.35	0.39	0.54	0.71	0.83	0.52	0.45	0.39	0.28	0.32	0.48	0.67	0.81
-0.30	0.71	0.68	0.60	0.52	0.47	0.53	0.66	0.79	0.73	0.65	0.58	0.46	0.39	0.40	0.53	0.69
-0.20	0.97	0.93	0.84	0.75	0.67	0.62	0.67	0.77	0.99	0.89	0.82	0.69	0.61	0.54	0.52	0.61
-0.10	1.25	1.21	1.11	1.03	0.94	0.83	0.77	0.80	1.27	1.17	1.10	0.96	0.88	0.81	0.72	0.67
-0.05	1.39	1.35	1.25	1.17	1.08	0.87	0.88	0.85	1.41	1.31	1.24	1.10	1.02	0.95	0.87	0.79
-0.01	1.49	1.46	1.35	1.27	1.18	1.08	0.98	0.93	1.50	1.42	1.34	1.21	1.13	1.06	0.98	0.90
0.01	1.99	1.96	1.86	1.77	1.68	1.57	1.45	1.33	2.00	1.92	1.84	1.71	1.63	1.56	1.48	1.39
0.05	1.95	1.91	1.81	1.73	1.64	1.52	1.39	1.27	1.97	1.87	1.80	1.66	1.58	1.51	1.43	1.33
0.10	1.87	1.84	1.74	1.65	1.56	1.45	1.31	1.19	1.89	1.80	1.72	1.59	1.51	1.43	1.35	1.24
0.20	1.71	1.68	1.58	1.50	1.41	1.29	1.18	1.10	1.73	1.64	1.57	1.44	1.35	1.27	1.19	1.11
0.30	1.55	1.52	1.43	1.35	1.27	1.18	1.10	1.06	1.57	1.48	1.42	1.29	1.21	1.14	1.09	1.05
0.40	1.40	1.38	1.30	1.23	1.17	1.10	1.06	1.03	1.42	1.34	1.29	1.17	1.11	1.06	1.04	1.02
0.50	1.28	1.26	1.20	1.14	1.10	1.06	1.03	1.02	1.29	1.23	1.18	1.09	1.05	1.03	1.01	1.01
0.60	1.18	1.17	1.12	1.08	1.05	1.03	1.02	1.01	1.19	1.14	1.10	1.03	1.02	1.01	1.00	1.00
0.70	1.10	1.10	1.06	1.04	1.02	1.01	1.01	1.00	1.10	1.07	1.05	1.01	1.00	1.00	1.00	1.00
0.80	1.05	1.05	1.03	1.01	1.01	1.00	1.00	1.00	1.05	1.03	1.01	1.00	1.00	1.00	1.00	1.00
0.90	1.02	1.02	1.00	1.00	1.00	1.00	1.00	1.00	1.01	1.00	1.00	1.00	1.00	1.00	1.00	1.00
W_R	-0.37	-0.35	-0.29	-0.24	-0.19	-0.14	-0.09	-0.06	-0.36	-0.32	-0.27	-0.20	-0.16	-0.12	-0.09	-0.06
W_B	0.49	0.47	0.42	0.36	0.31	0.25	0.18	0.12	0.50	0.45	0.40	0.32	0.27	0.23	0.19	0.15
W_T	0.12	0.13	0.13	0.13	0.12	0.11	0.08	0.06	0.13	0.13	0.13	0.12	0.12	0.11	0.10	0.08
$-W_R/W_B$	0.75	0.73	0.69	0.66	0.62	0.57	0.52	0.50	0.73	0.71	0.68	0.62	0.57	0.52	0.48	0.43

TABLE 5

LINE PROFILES FOR $w = 0.01 + 0.99(1 - x^{-1})^4$, $\tau(w)$ FROM EQUATION (8)

	$\beta = 4$	$\gamma = 0.5$							$\beta = 4$	$\gamma = 1$						
v/v_∞	$T=10^3$	10	4	2	1	0.5	0.25	0.1	10^3	10	4	2	1	0.5	0.25	0.10
-0.95	0.00	0.00	0.22	0.49	0.70	0.84	0.92	0.97	0.00	0.33	0.65	0.81	0.90	0.95	0.98	0.99
-0.90	0.03	0.05	0.19	0.41	0.64	0.80	0.89	0.96	0.03	0.17	0.47	0.68	0.82	0.91	0.96	0.98
-0.80	0.05	0.07	0.14	0.31	0.54	0.74	0.86	0.94	0.05	0.08	0.25	0.48	0.68	0.83	0.91	0.97
-0.70	0.11	0.13	0.16	0.30	0.50	0.71	0.84	0.93	0.11	0.12	0.18	0.37	0.59	0.76	0.87	0.95
-0.60	0.20	0.20	0.22	0.32	0.50	0.69	0.82	0.92	0.20	0.19	0.21	0.33	0.53	0.71	0.84	0.94
-0.50	0.31	0.31	0.30	0.37	0.52	0.69	0.82	0.92	0.31	0.29	0.27	0.33	0.50	0.68	0.82	0.92
-0.40	0.47	0.45	0.43	0.45	0.56	0.72	0.83	0.93	0.47	0.43	0.38	0.39	0.51	0.67	0.82	0.92
-0.30	0.67	0.64	0.60	0.59	0.65	0.75	0.86	0.94	0.67	0.62	0.56	0.52	0.57	0.69	0.82	0.92
-0.20	0.93	0.90	0.85	0.79	0.78	0.83	0.89	0.95	0.93	0.87	0.81	0.73	0.70	0.76	0.85	0.93
-0.10	1.30	1.26	1.21	1.13	1.03	0.98	0.98	0.99	1.30	1.23	1.16	1.07	0.96	0.91	0.93	0.96
-0.05	1.58	1.54	1.49	1.39	1.24	1.13	1.06	1.03	1.58	1.51	1.44	1.34	1.19	1.08	1.03	1.01
-0.01	1.98	1.93	1.88	1.77	1.58	1.40	1.25	1.12	1.97	1.90	1.83	1.73	1.54	1.38	1.24	1.12
0.01	2.72	2.68	2.63	2.50	2.22	1.87	1.55	1.26	2.72	2.65	2.58	2.47	2.24	1.93	1.61	1.30
0.05	2.45	2.40	2.35	2.22	1.95	1.63	1.37	1.17	2.44	2.37	2.31	2.19	1.97	1.67	1.40	1.18
0.10	2.22	2.18	2.12	2.00	1.76	1.48	1.28	1.12	2.21	2.14	2.08	1.97	1.75	1.50	1.29	1.13
0.20	1.89	1.85	1.81	1.70	1.51	1.32	1.18	1.08	1.88	1.82	1.76	1.66	1.48	1.30	1.17	1.08
0.30	1.64	1.62	1.58	1.49	1.35	1.22	1.12	1.05	1.64	1.59	1.54	1.45	1.32	1.20	1.11	1.05
0.40	1.46	1.44	1.41	1.35	1.25	1.15	1.09	1.04	1.45	1.42	1.37	1.30	1.21	1.13	1.07	1.03
0.50	1.31	1.30	1.29	1.24	1.17	1.10	1.06	1.03	1.31	1.28	1.25	1.20	1.13	1.08	1.04	1.02
0.60	1.19	1.20	1.19	1.16	1.11	1.07	1.04	1.02	1.19	1.18	1.16	1.12	1.08	1.05	1.03	1.01
0.70	1.11	1.12	1.12	1.10	1.07	1.04	1.02	1.01	1.11	1.11	1.10	1.07	1.04	1.03	1.01	1.01
0.80	1.05	1.07	1.07	1.06	1.04	1.02	1.01	1.01	1.05	1.06	1.05	1.03	1.02	1.01	1.01	1.00
0.90	1.01	1.03	1.03	1.02	1.01	1.01	1.00	1.00	1.01	1.02	1.02	1.01	1.01	1.00	1.00	1.00
W_R	-0.45	-0.45	-0.42	-0.37	-0.27	-0.17	-0.10	-0.04	-0.45	-0.43	-0.39	-0.34	-0.25	-0.16	-0.10	-0.04
W_B	0.52	0.52	0.49	0.43	0.32	0.20	0.12	0.05	0.52	0.49	0.45	0.39	0.30	0.20	0.12	0.05
W_T	0.07	0.07	0.07	0.06	0.05	0.03	0.02	0.01	0.07	0.06	0.06	0.05	0.05	0.03	0.02	0.01
$-W_R/W_B$	0.87	0.86	0.86	0.86	0.86	0.85	0.84	0.86	0.87	0.87	0.87	0.86	0.84	0.83	0.82	0.84

TABLE 5—*Continued*

v/v_∞	$\beta = 4$ $\gamma = 2$ T=10^3	10^2	10	4	2	1	0.5	0.25	$\beta = 4$ $\gamma = 4$ 10^6	10^3	10^2	10	4	2	1	0.5
-0.95	0.00	0.44	0.92	0.97	0.99	1.00	1.00	1.00	0.00	0.97	1.00	1.00	1.00	1.00	1.00	1.00
-0.90	0.04	0.08	0.74	0.89	0.95	0.97	0.99	1.00	0.03	0.61	0.95	1.00	1.00	1.00	1.00	1.00
-0.80	0.05	0.05	0.32	0.63	0.79	0.89	0.95	0.97	0.05	0.04	0.45	0.93	0.97	0.99	1.00	1.00
-0.70	0.11	0.11	0.14	0.38	0.60	0.78	0.88	0.94	0.11	0.08	0.07	0.68	0.85	0.93	0.96	0.98
-0.60	0.19	0.18	0.15	0.24	0.45	0.65	0.81	0.90	0.19	0.15	0.12	0.33	0.62	0.79	0.88	0.94
-0.50	0.30	0.28	0.23	0.23	0.35	0.55	0.73	0.85	0.30	0.25	0.21	0.17	0.36	0.58	0.75	0.87
-0.40	0.46	0.43	0.36	0.31	0.34	0.49	0.67	0.81	0.46	0.40	0.35	0.25	0.25	0.38	0.59	0.76
-0.30	0.65	0.62	0.54	0.47	0.42	0.49	0.64	0.78	0.66	0.59	0.53	0.41	0.34	0.34	0.45	0.63
-0.20	0.91	0.88	0.79	0.71	0.63	0.59	0.66	0.77	0.92	0.84	0.78	0.65	0.57	0.49	0.47	0.57
-0.10	1.28	1.25	1.15	1.07	0.97	0.86	0.81	0.84	1.29	1.21	1.14	1.01	0.93	0.84	0.73	0.68
-0.05	1.56	1.52	1.43	1.35	1.25	1.12	1.00	0.95	1.56	1.49	1.42	1.28	1.20	1.12	1.01	0.90
-0.01	1.95	1.92	1.82	1.74	1.64	1.49	1.33	1.21	1.96	1.88	1.81	1.67	1.59	1.51	1.40	1.26
0.01	2.70	2.67	2.57	2.49	2.39	2.22	1.97	1.69	2.71	2.63	2.56	2.43	2.34	2.26	2.14	1.97
0.05	2.42	2.39	2.29	2.21	2.11	1.94	1.70	1.44	2.43	2.35	2.28	2.15	2.07	1.98	1.86	1.68
0.10	2.20	2.16	2.06	1.98	1.88	1.72	1.49	1.30	2.20	2.12	2.05	1.92	1.84	1.75	1.63	1.45
0.20	1.87	1.84	1.74	1.67	1.57	1.42	1.27	1.15	1.87	1.80	1.73	1.61	1.53	1.44	1.32	1.20
0.30	1.63	1.60	1.52	1.45	1.36	1.25	1.15	1.09	1.63	1.56	1.50	1.39	1.31	1.23	1.15	1.09
0.40	1.44	1.42	1.35	1.29	1.22	1.14	1.08	1.05	1.44	1.38	1.33	1.23	1.16	1.11	1.06	1.04
0.50	1.30	1.28	1.22	1.18	1.13	1.08	1.04	1.02	1.30	1.25	1.20	1.12	1.07	1.04	1.02	1.01
0.60	1.19	1.18	1.14	1.10	1.07	1.04	1.02	1.01	1.19	1.15	1.11	1.05	1.03	1.01	1.01	1.00
0.70	1.11	1.10	1.07	1.05	1.03	1.02	1.01	1.00	1.10	1.08	1.06	1.01	1.01	1.00	1.00	1.00
0.80	1.05	1.05	1.03	1.02	1.01	1.01	1.00	1.00	1.05	1.04	1.01	1.00	1.00	1.00	1.00	1.00
0.90	1.02	1.02	1.01	1.00	1.00	1.00	1.00	1.00	1.02	1.00	1.00	1.00	1.00	1.00	1.00	1.00
W_R	-0.45	-0.43	-0.37	-0.33	-0.28	-0.21	-0.14	-0.09	-0.44	-0.40	-0.36	-0.29	-0.25	-0.21	-0.16	-0.12
W_B	0.50	0.48	0.43	0.38	0.33	0.26	0.18	0.11	0.50	0.46	0.42	0.34	0.29	0.25	0.21	0.15
W_T	0.06	0.06	0.06	0.05	0.05	0.05	0.04	0.02	0.05	0.06	0.06	0.05	0.05	0.05	0.04	0.04
$-W_R/W_B$	0.89	0.88	0.87	0.86	0.85	0.83	0.80	0.78	0.90	0.88	0.87	0.85	0.84	0.82	0.79	0.76

TABLE 6

LINE PROFILES FOR $w = 0.01 + 0.99(1 - x^{-1})^{1/2}$, $\tau(w)$ FROM EQUATION (15)

	$w_{min} = 0.01$								$w_{max} = 0.50$							
	$\gamma = 0$					$\gamma = 1$					$\gamma = 2$					
v/v_∞	T=10	4	1	0.4	0.1	40	4	1	0.4	0.1	10^3	10	4	1	0.4	0.1
-0.50	1.00	1.00	1.00	1.00	1.00	1.00	1.00	1.00	1.00	1.00	1.00	1.00	1.00	1.00	1.00	1.00
-0.475	0.64	0.64	0.69	0.81	0.94	0.64	0.89	0.97	0.99	1.00	0.72	0.98	0.99	1.00	1.00	1.00
-0.45	0.31	0.31	0.40	0.62	0.88	0.31	0.65	0.88	0.95	0.99	0.38	0.88	0.95	0.99	1.00	1.00
-0.40	0.14	0.14	0.24	0.50	0.84	0.14	0.25	0.64	0.83	0.95	0.13	0.46	0.70	0.91	0.96	0.99
-0.35	0.21	0.22	0.29	0.54	0.84	0.21	0.21	0.49	0.73	0.92	0.20	0.21	0.40	0.76	0.89	0.97
-0.30	0.31	0.31	0.38	0.58	0.85	0.31	0.28	0.41	0.65	0.89	0.31	0.25	0.28	0.59	0.80	0.94
-0.25	0.42	0.42	0.46	0.62	0.87	0.42	0.39	0.41	0.61	0.87	0.42	0.36	0.33	0.47	0.70	0.91
-0.20	0.54	0.54	0.56	0.67	0.89	0.54	0.51	0.47	0.59	0.84	0.54	0.48	0.45	0.44	0.61	0.87
-0.15	0.68	0.68	0.68	0.74	0.89	0.68	0.65	0.57	0.61	0.83	0.67	0.62	0.58	0.50	0.57	0.82
-0.10	0.81	0.81	0.80	0.81	0.91	0.81	0.79	0.71	0.68	0.83	0.81	0.76	0.73	0.64	0.61	0.78
-0.05	0.95	0.95	0.94	0.91	0.95	0.95	0.92	0.85	0.79	0.84	0.95	0.90	0.86	0.79	0.72	0.77
-0.01	1.06	1.06	1.04	1.01	1.01	1.06	1.03	0.96	0.89	0.90	1.05	1.00	0.97	0.89	0.83	0.83
0.01	1.56	1.56	1.52	1.42	1.23	1.56	1.53	1.46	1.36	1.22	1.55	1.50	1.47	1.39	1.32	1.20
0.05	1.51	1.51	1.48	1.36	1.15	1.51	1.48	1.41	1.31	1.14	1.51	1.46	1.42	1.34	1.26	1.12
0.10	1.44	1.44	1.41	1.29	1.11	1.44	1.41	1.33	1.22	1.08	1.44	1.38	1.35	1.26	1.17	1.06
0.15	1.36	1.36	1.33	1.22	1.08	1.36	1.34	1.25	1.15	1.05	1.36	1.31	1.27	1.17	1.09	1.03
0.20	1.29	1.29	1.26	1.17	1.06	1.29	1.26	1.17	1.09	1.03	1.28	1.23	1.19	1.10	1.05	1.01
0.25	1.21	1.21	1.19	1.12	1.04	1.21	1.18	1.11	1.05	1.02	1.21	1.15	1.11	1.05	1.02	1.01
0.30	1.14	1.14	1.12	1.08	1.03	1.14	1.11	1.06	1.03	1.01	1.14	1.08	1.05	1.02	1.01	1.00
0.35	1.08	1.08	1.07	1.04	1.01	1.08	1.05	1.02	1.01	1.00	1.08	1.03	1.01	1.00	1.00	1.00
0.40	1.03	1.03	1.03	1.02	1.01	1.03	1.01	1.00	1.00	1.00	1.03	1.00	1.00	1.00	1.00	1.00
0.45	1.00	1.00	1.00	1.00	1.00	1.00	1.00	1.00	1.00	1.00	1.00	1.00	1.00	1.00	1.00	1.00

TABLE 6—*Continued*

w_{min} = 0.50 w_{max} = 1.00

v/v_∞	γ = 0 T=10	γ = 0 4	γ = 0 1	γ = 0 0.4	γ = 0 0.1	γ = 1 10	γ = 1 4	γ = 1 1	γ = 1 0.4	γ = 1 0.1	γ = 2 10^3	γ = 2 10	γ = 2 4	γ = 2 1	γ = 2 0.4	γ = 2 0.1
-0.95	0.01	0.02	0.16	0.47	0.83	0.04	0.23	0.68	0.86	0.97	0.01	0.57	0.80	0.95	0.98	1.00
-0.90	0.02	0.03	0.17	0.49	0.83	0.03	0.08	0.49	0.75	0.93	0.02	0.13	0.43	0.81	0.92	0.98
-0.80	0.05	0.06	0.23	0.52	0.85	0.06	0.07	0.28	0.59	0.87	0.05	0.05	0.09	0.46	0.73	0.92
-0.70	0.12	0.13	0.28	0.57	0.86	0.12	0.13	0.22	0.49	0.83	0.12	0.11	0.10	0.23	0.52	0.85
-0.60	0.21	0.21	0.35	0.60	0.87	0.21	0.20	0.23	0.43	0.79	0.21	0.19	0.18	0.18	0.36	0.75
-0.50	0.39	0.39	0.48	0.68	0.89	0.39	0.38	0.35	0.45	0.78	0.39	0.36	0.35	0.29	0.35	0.69
-0.45	1.13	1.13	1.11	1.07	1.06	1.12	1.11	1.05	1.01	1.00	1.13	1.10	1.08	1.02	0.97	0.97
-0.40	1.38	1.37	1.31	1.20	1.07	1.37	1.35	1.29	1.20	1.07	1.38	1.34	1.32	1.26	1.18	1.07
-0.30	1.41	1.40	1.32	1.20	1.07	1.40	1.38	1.30	1.20	1.07	1.41	1.37	1.34	1.27	1.19	1.07
-0.20	1.42	1.41	1.33	1.20	1.07	1.41	1.39	1.31	1.20	1.07	1.43	1.38	1.35	1.27	1.19	1.07
-0.10	1.44	1.42	1.33	1.20	1.07	1.42	1.40	1.32	1.20	1.07	1.45	1.39	1.36	1.28	1.19	1.07
0.00	1.44	1.42	1.33	1.20	1.07	1.42	1.40	1.32	1.20	1.07	1.45	1.39	1.36	1.28	1.19	1.07
0.10	1.44	1.42	1.33	1.20	1.07	1.42	1.40	1.32	1.20	1.07	1.45	1.39	1.36	1.28	1.19	1.07
0.20	1.42	1.41	1.33	1.20	1.07	1.41	1.39	1.31	1.20	1.07	1.43	1.38	1.35	1.27	1.19	1.07
0.30	1.41	1.40	1.32	1.20	1.07	1.40	1.38	1.30	1.20	1.07	1.41	1.37	1.34	1.27	1.19	1.07
0.40	1.38	1.37	1.31	1.20	1.07	1.37	1.35	1.29	1.20	1.07	1.38	1.34	1.32	1.26	1.18	1.07
0.50	1.29	1.29	1.25	1.16	1.05	1.28	1.27	1.22	1.15	1.05	1.29	1.26	1.24	1.19	1.13	1.05
0.60	1.18	1.19	1.18	1.12	1.04	1.18	1.18	1.15	1.09	1.03	1.18	1.17	1.15	1.11	1.07	1.02
0.70	1.11	1.12	1.12	1.08	1.03	1.11	1.11	1.09	1.05	1.02	1.10	1.10	1.09	1.06	1.03	1.01
0.80	1.05	1.06	1.07	1.05	1.02	1.06	1.06	1.04	1.03	1.01	1.05	1.05	1.04	1.02	1.01	1.00
0.90	1.02	1.02	1.03	1.02	1.01	1.03	1.03	1.01	1.01	1.00	1.02	1.02	1.01	1.00	1.00	1.00

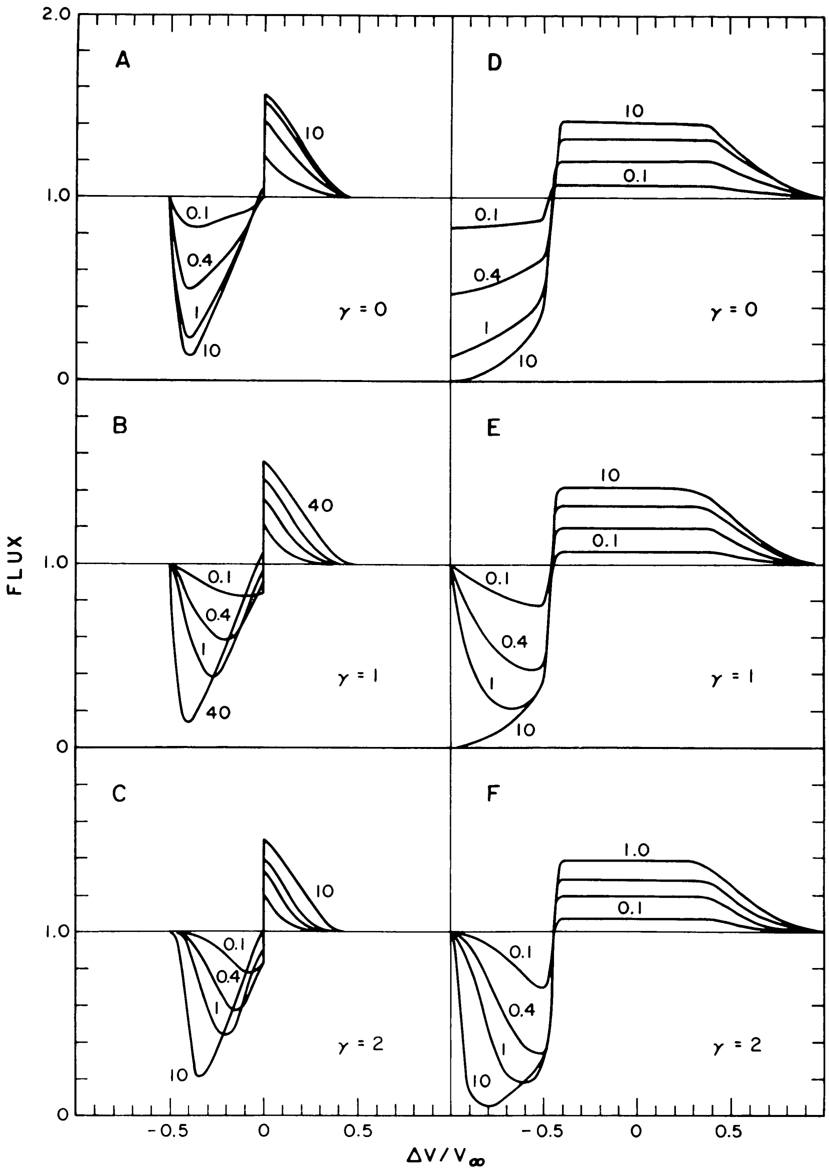

FIG. 10.—Profiles on the hypothesis that the absorbing ion is absent from part of the envelope. The ion is present (*a*)–(*c*) between $w_{\min} = 0.01$ and $w_{\max} = 0.50$, and (*d*)–(*f*) between $w_{\min} = 0.50$ and $w_{\max} = 1.00$. The optical depth $\tau(w)$ was given by eq. (15) with the value of γ indicated in each panel. The total optical depth $\mathcal{T}$ is shown next to each profile. The velocity law was eq. (4) with $\beta = \frac{1}{2}$.

condition, using Lucy's method. The photospheric spectrum was assumed to be a continuum with a strong absorption line that had a Lorentz profile with a FWHM of $0.60 \times v_\infty$. The residual intensity $r = F_\nu/F_c$ of the resulting profile is shown in Figure 13 for two different $\tau(v)$ relations in the envelope. For comparison we also plot the adopted photospheric profile r_{phot} and the envelope profile r_{env} for the same $\tau(v)$ relation if the photospheric spectrum is a continuum. It is easy to check that the resulting profile cannot be considered as a linear superposition of the envelope profile and the photospheric profile.

We found instead that the profile can be approximated with reasonable accuracy by the following expressions:

$$r(\Delta v) = r_{\text{phot}}(\Delta v) + q[r_{\text{env}}(\Delta v) - 1] \tag{19a}$$

for the long-wavelength side of the profile ($\Delta v > 0$), and

$$r(\Delta v) = r_{\text{phot}}(\Delta v)\{r_{\text{env}}(\Delta v) - [r_{\text{env}}(-\Delta v) - 1]\} + [r_{\text{env}}(-\Delta v) - 1]q \tag{19b}$$

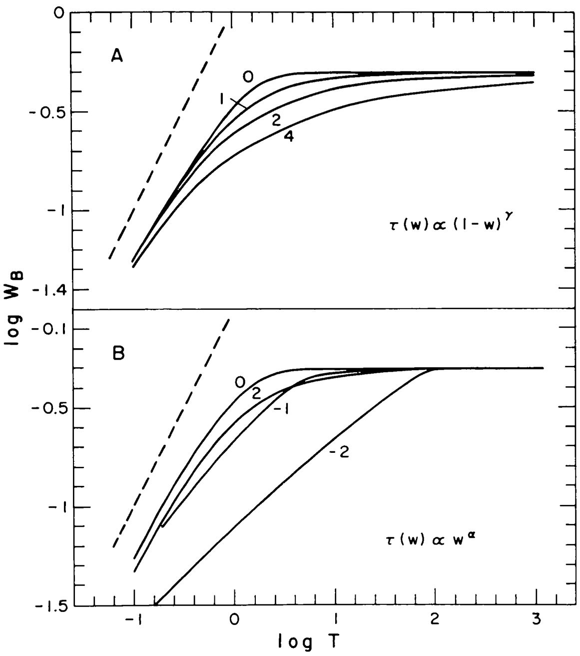

FIG. 11.—Curves of growth for the short-wavelength side of the P Cygni profiles. The curves are for (*a*) $\tau \propto (1 - w)^{\gamma}$ and (*b*) $\tau \propto w^{\alpha}$. The curves are labeled with their values of α and γ. The dashed line is the linear part of the curve of growth for pure absorption in a plane-parallel atmosphere for a Planck function proportional to optical depth and a thermal velocity of v_∞.

for the short-wavelength side of the profile ($\Delta v \leq 0$), where

$$q = \int_{\Delta v = -v_\infty}^{\Delta v = 0} r_{\rm phot}(\Delta v) d(\Delta v / v_\infty) . \qquad (19c)$$

This approximation is also shown in Figure 13, and we see that even for a very strong photospheric profile the approximation is reasonably accurate.

The approximation can be understood as follows: The P Cygni profile consists of the sum of a shortward shifted absorption, produced in the part of the envelope that is seen projected against the stellar disk, and an emission that is symmetrical around $\Delta v = 0$, produced by photons that are scattered by the envelope into the line of sight. If the photospheric spectrum contains an absorption profile, the amount of photospheric radiation that can be scattered into the line of sight is reduced by a factor q, the mean photospheric flux in the wavelength interval corresponding to $\Delta v = -v_\infty$ to $\Delta v = +v_\infty$; thus the long-wavelength emission is reduced by a factor q (second term of eq. [19a]). On the short-wavelength side, the reduction factor $r_{\rm env}(\Delta v) - r_{\rm env}(-\Delta v) + 1$ that accounts for envelope absorption is impressed on the photospheric profile before the reduced emission is added.

These approximations allow the envelope contribution to be retrieved from an observed profile if the photospheric profile is known; alternatively, the calculated P Cygni profiles in this atlas can be corrected for the photospheric profile and compared with the observations. As the figure shows, the corrections can be quite large.

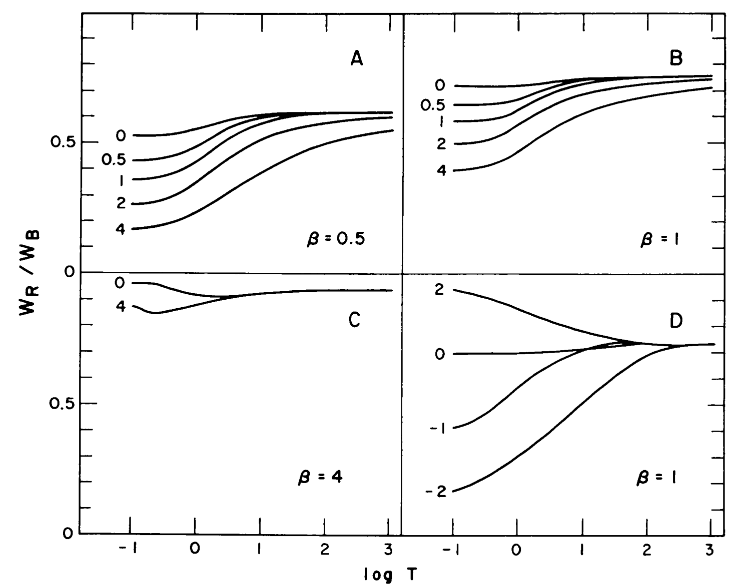

FIG. 12.—Ratio of the emission equivalent width W_R of the red (long-wavelength) component to the absorption equivalent width W_B of the blue (short-wavelength) component of the P Cygni profiles. W_B includes all frequencies shortward of line center, and W_R includes all frequencies longward of line center. The abscissa is the total optical depth given by eq. (9). Panels (*a*), (*b*), and (*c*) are for the optical depth law eq. (8) with the value of γ shown on each curve. Panel (*d*) is for the optical depth law eq. (7) with α shown on the curves. In all cases the velocity law was eq. (4) and the value of β is indicated for each panel.

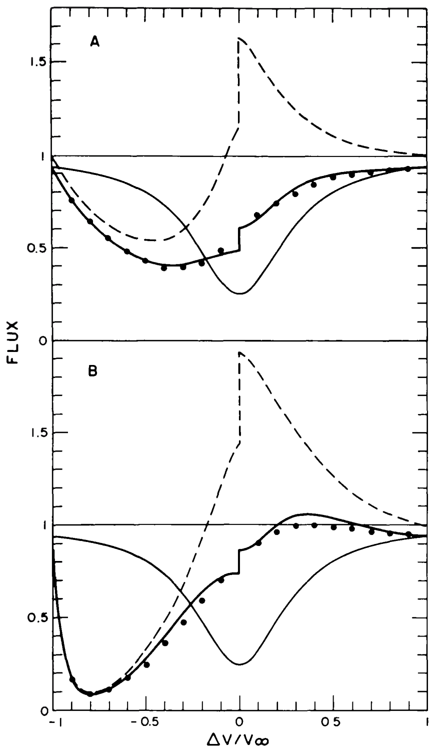

FIG. 13.—Correction of the envelope profile for the presence of a photospheric absorption line. The profiles are calculated with a velocity law $w = 0.01 + 0.99[1 - (1/x)]$ and an optical depth law $\tau(w) \propto 1 - w$. The total optical depth is (*a*) $\mathscr{T} = 1$ and (*b*) $\mathscr{T} = 10$. The dashed lines show the envelope profiles for a photosphere emitting a continuous spectrum. The thick solid line shows the resulting profile for a photospheric spectrum having an absorption line (*thin solid line*). The dots show the approximation to the resulting profile, derived from the envelope profile and the photospheric profile by means of eq. (19).

VI. EFFECT OF COLLISIONAL EXCITATION

We mentioned in § III that the assumption of conservative scattering in the line will break down if $\epsilon\tau$ is sufficiently large. Since ϵ is itself very small (no larger than 10^{-5}) for resonance lines, collisional excitation will be important only for lines that are very optically thick. In this case the expression

$$S = \frac{\beta_c I_c + \epsilon B_\nu}{\beta + \epsilon} \tag{20}$$

given by Castor (1970) for the line source function becomes

$$S = \frac{W[1 + (\sigma/3)(1 + X + X^2)]I_c + \epsilon\tau_0 B_\nu}{1 + (\sigma/3) + \epsilon\tau_0} \tag{21}$$

($\sigma = d \ln w/d \ln x - 1$, $X = [1 - (R_*/r)^2]^{1/2}$, $W = (1 - X)/2$). The quantity τ_0 that appears here is the *tangential* optical depth, related to the radial optical depth by $\tau_0 = \tau_{\rm rad} d \ln w/d \ln x$. Evidently the source function, and therefore also the profile, is determined by the velocity law, the temperature distribution, and the run of $\epsilon\tau_0$. By combining equation (1) for $\tau_{\rm rad}$ and equation (12) for ϵ, we arrive at the following expression for $\epsilon\tau_0$:

$$\epsilon\tau_0 = \frac{C}{(wx)^3}, \tag{22}$$

where C is given by

$$C = 6.5 \times 10^3 \frac{(\lambda_{1000})^4}{T_4^{1/2}} f_{12} f_i A \times \frac{(\dot{\mathfrak{M}}_5)^2}{(v_8 R_{12})^3}\left[1 - \exp\left(-\frac{\chi_{12}}{kT_e}\right)\right], \tag{23}$$

in which f_{12} is the oscillator strength, λ_{1000} is the wavelength in units of 1000 Å, T_4 is the electron temperature in 10^4 K, f_i is the fractional ionic abundance, A is the element abundance by number relative to the total number of ions, $\dot{\mathfrak{M}}_5$ is the rate of mass loss in $10^{-5}\,\mathfrak{M}_\odot$ year^{-1}, v_8 is the terminal velocity in 1000 km s^{-1}, and R_{12} is the stellar radius in 10^{12} cm.

We have illustrated the effect of collisions by using equation (21) to compute line profiles for several different values of C and B_ν/I_c. The velocity law was taken to be the $\beta = \frac{1}{2}$ case, $w = (1 - 1/x)^{1/2}$. Constant values were taken for C and B_ν/I_c corresponding to constant temperature and ionization fraction. The profiles are shown in Figure 14.

It is apparent that the profile begins to differ significantly from the conservative case (shown as

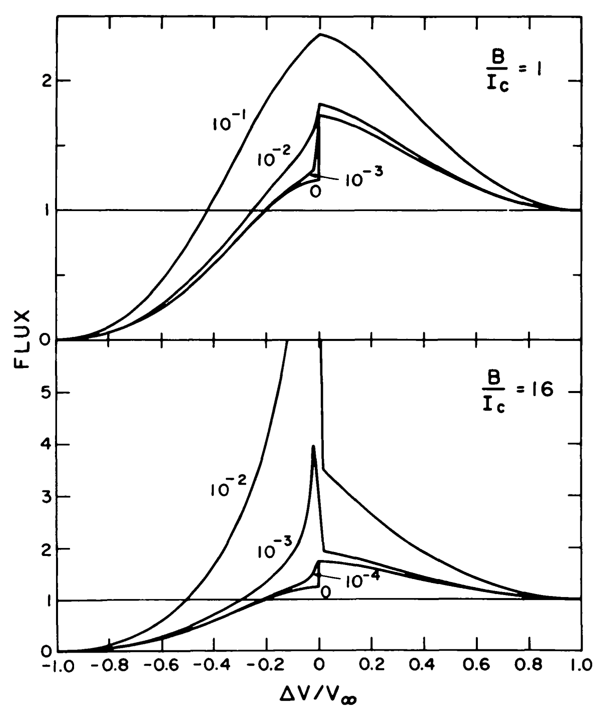

FIG. 14.—Profiles including the effect of collisional excitation in the line. The velocity law is $w = [1 - (1/x)]^{1/2}$. Large optical depth is assumed, and the profiles are determined by $\epsilon\tau_0$, which is taken to be $\epsilon\tau_0 = C/(wx)^3$. The value of C is indicated by each profile. *Upper panel*, $B_\nu(T_e) = I_c$, the continuum intensity; *lower panel*, $B_\nu(T_e) = 16I_c$.

$C = 0$) when C is still fairly small, and it is also apparent that for the hot envelope ($B/I_c = 16$) the changes in the profile are rather dramatic. The profile changes are due to extra emission created by the collisions. Since $\epsilon\tau_0$ is so strongly dependent on radius, this extra emission is strong in the low-velocity region and weak farther out. This explains why the emission is greatest near line center, and it also explains why the blue side is affected more strongly than the red side—the low-velocity region is largely occulted on the red side of the profile. The extra emission is proportional to B_ν, and thus is much stronger for $B/I_c = 16$ than for $B = I_c$.

Formula (23) implies that in a lucky case for which $\dot{\mathfrak{M}}$ was large; v_∞ and R were small; and λ, f_{12}, f_l, and A were large; C could be as large as 2×10^{-3} or so. (This may apply, for example, to P Cyg.) This would produce easily detected changes in the profile if $B/I_c = 16$ but not if $B = I_c$. For a more typical combination of parameters, C is 10^{-4} or less, and no effects could be detected. (Changes in the profile very close to line center are modified a great deal by the error in the Sobolev approximation and by photospheric absorption, as we have already discussed.)

We conclude that for the normal line in the normal star collisional excitation is not important, but for the strongest lines in stars with very intense winds it could be an important effect and should be remembered.

VII. FORMATION OF DOUBLETS

Many of the ultraviolet resonance lines in the spectra of early-type stars are doublets with a separation smaller than their widths, which results in partly overlapping lines. One of the authors (J. I. C.) has adapted the escape probability method to solve the transfer equations for doublets. The calculations show that the doublet profile differs strongly from the profile obtained by a simple addition or superposition of two separately calculated components. This is due to the fact that radiation scattered by the blue component in the direction of the observer can be scattered again by the red component. So the radiation scattered by both components appears as an enhancement of the emission on the long-wavelength side of the red component.

In principle, the doublet profiles can be computed for any velocity law, optical depth law, and separation of the components. For the purpose of comparing observed profiles with those presented in this atlas, it is useful to have a simple method for deriving the profile of the doublet from the profiles of the two separate components. Let $r^B(v)$ and $r^R(v)$ be the flux of the blue and red components relative to the continuum if calculated separately, and let $r^D(v)$ be the flux profile of the doublet. The velocity v is the Doppler velocity corresponding to the shift relative to the wavelength $\lambda_0{}^R$ of the undisplaced *red* component:

$$v = c(\lambda/\lambda_0{}^R - 1)\,. \qquad (24)$$

Let $\tau^R(v)$ be the optical depth of the red component. The profile of the doublet can be approximated by

$$r^D(v) \approx r^R(v) + [r^B(v) - 1] \exp[-\tau^R(|v|)] + QR(v) \qquad (25)$$

with

$$Q = \int_{-v_\infty}^{v_\infty} [r^B(v) - 1]\{1 - \exp[-\tau^R(|v|)]\}dv \qquad (26)$$

and

$$R(v) = [r^R(|v|) - 1]/2\int_0^{v_\infty} [r^R(|v|) - 1]dv\,. \qquad (27)$$

The first term of equation (25) is the profile of the red component, which is not affected by the presence of a blue component. The second term is the contribution of the blue component reduced by a factor $\exp(-\tau^R)$ due to scattering in the red component. The third term is the radiation from the blue component which is scattered and redistributed over frequency by the red component. The factor Q is the amount of scattered radiation, i.e., the complement of the second term integrated over the velocities in the region where the lines overlap. The function $R(v)$ describes the redistribution of the radiation Q over frequency or velocity in the profile. We assume that this redistribution is the same as the distribution of the emission, $r^R(|v|) - 1$, of the red component. This method is demonstrated in Figure 15; its accuracy is shown in Figure 16, where the approximate doublet profile is compared with the exact solutions for optically thin and optically thick lines (Castor 1979).

A few properties of the doublets, derived from equation (25), are worth mentioning: (i) At short wavelengths where the blue component is not overlapped by the red component, we find $v < -v_\infty$, $r^R(v) = 1$, $\tau^R(|v|) = 0$, and $R(v) = 0$; so $r^D(v) = r^B(v)$, which is the undisturbed part of the blue component. (ii) If the separation of the components is larger than $2v_\infty$ so that there is no overlap at all, we find $r^R(v) = 1$ and $\tau^R(|v|) = 0$ in the wavelength range of the blue profile and $r^B(v) = 1$ and $Q = 0$ in the range of the red profile. Consequently, we retrieve the two undisturbed profiles. (iii) The discontinuity at the rest wavelength $\lambda_0{}^B$ of the blue line will be reduced by a factor $\exp[-\tau^R(|v'|)]$ in the doublet profile, where v' is the velocity corresponding to a wavelength shift of $\lambda_0{}^B - \lambda_0{}^R$. So if the red component is optically thick, this discontinuity will not be visible in the doublet.

VIII. CONCLUSIONS

We have presented an atlas of Beals (1951) type I P Cygni profiles, that is, profiles with short-wavelength absorption and long-wavelength emission. These are profiles of lines formed by resonance fluorescence in a spherically expanding stellar envelope; photons that originate in the continuum of the star scatter repeatedly until they escape. The probability that a photon will

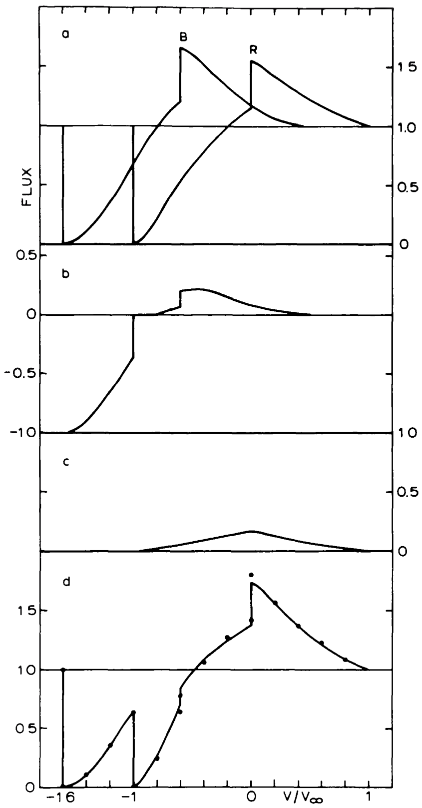

FIG. 15.—Method for estimating the profiles of doublets. (*a*) Profiles of the two components calculated separately. The blue (*B*) and red (*R*) components are calculated with $\tau^B = 1.5/(1 - w^2)$, $\tau^R = 0.75/(1 - w^2)$, and $w = [1 - (1/x)]^{0.5}$. (*b*) Contribution of the blue component reduced by a factor $\exp(-\tau^R|v|)$. (*c*) Radiation from the blue component that is scattered and redistributed by the red component. (*d*) Resulting (*dots*) approximate doublet profile calculated by means of eq. (25), and (*solid line*) exact profile calculated with the escape probability method for doublets.

be destroyed in the course of scattering is negligible because of the low density in the envelope. We have presented profiles computed for a range of nondimensional velocity functions $w(x)$ and local optical depth functions $\tau(w)$, where $w = v/v_\infty$ and $x = r/R_*$.

Accurate observations of a P Cygni–type profile supply two functions of the scaled velocity w, namely, the fluxes at the displacement w in either direction from line center. Therefore, it should be possible in principle to derive both the velocity law and the optical depth function from a single line profile. In practice, the computed profiles have shown us that the short-wavelength wing of the line is sensitive primarily to $\tau(w)$ and not sensitive at all to $w(x)$, while the long-wavelength wing is sensitive to both. Furthermore, the sensitivity of the long-wavelength wing to the velocity law is large only near the center of the line and vanishes toward the extreme. The central part of the profile is afflicted with uncertainties due to the underlying photospheric profile and the error of the Sobolev approximation.[1] Thus observations readily yield only

[1] The Sobolev approximation is valid in the case of a rapidly rising velocity law where $v \gtrsim 2v_{\mathrm{thermal}}$.

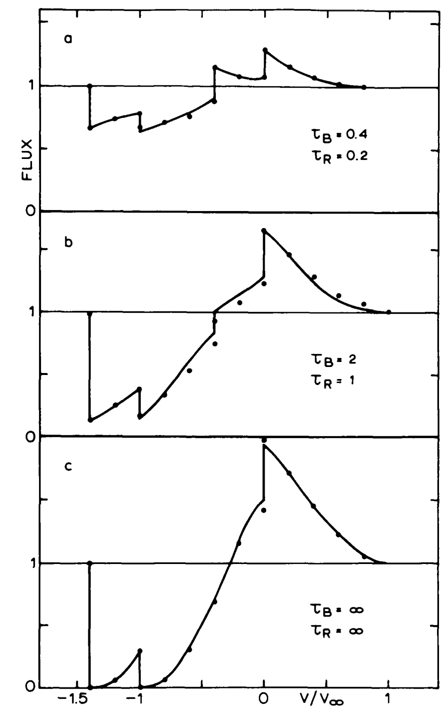

FIG. 16.—Comparison between (*dots*) approximate and (*solid lines*) exact doublet profiles for optically thin and optically thick lines and a velocity law of $w = [1 - (1/x)]^{0.5}$. The profiles are calculated with constant τ as indicated in the figure. The rest wavelengths of the lines are spaced by 0.4 $\lambda v_\infty/c$.

the optical depth law $\tau(w)$ for velocities in the range $0.25 \lesssim w < 1$. If the central part of the profile can be corrected sufficiently for the problems mentioned above, then the total amount of emission on the long-wavelength side of the profile can be used to distinguish between a slowly rising $w(x)$ and a steeply rising one. Finer discrimination of the velocity law than this may not be possible.

The variations with radius of the velocity w and the ion density n_i are inextricably entwined in the optical depth law (eq. [1]). For example, suppose that the ion density varies with radius as $n_i \propto w^p(1 - w)^q x^{-2}$ while the velocity varies as $w = (1 - x^{-\delta})^\beta$. Then the optical depth function is proportional to $w^{p+1/\beta-1}(1 - w)^q \times (1 - w^{1/\beta})^{1/\delta-1}$. When w is small the optical depth varies as $w^{p+1/\beta-1}$, while when w approaches 1 it varies as $(1 - w)^{q+1/\delta-1}$. Thus $n_i \propto w^{-1}x^{-2}$ and $w = (1 - 1/x)^{1/2}$ cannot be distinguished from $n_i \propto x^{-2}$ and $w = (1 - 1/x)$, nor can $n_i \propto (1 - w)x^{-2}$ and $w = (1 - 1/x)$ be distinguished from $n_i \propto x^{-2}$ and $w = 1 - x^{-1/2}$. The difficulty one faces in attempting to determine the velocity law by comparing profiles for a given optical depth law is evident from Figure 3. (Remember that the central part of the profile is nearly unusable!) It is essential for a proper determination of the variation of ionization with radius to find the correct velocity law. This might be done with the carefully corrected central part of a P Cygni profile (viz., § V) or with other data entirely.

Users of our profiles are advised to heed three cautions: (1) The profiles within a few tens of kilometers per second of the line center are wrong because of the Sobolev approximation; this problem is irremediable. (2) The profiles require correction for the underlying photospheric absorption within a few hundred kilometers per second of line center. This correction is certainly *not* additive, and the procedure of § V, while not exact, is certainly to be preferred to simple addition. The photospheric profiles themselves are a major uncertainty in this correction procedure. The resonance lines are affected by strong non–LTE effects even in the deeper part of the atmosphere, and good profile tabulations for most of the lines of interest do not now exist. (3) Saturated lines yield little information. In contrast to the case for static atmospheres, for which the profile continues to change no matter how large τ become the P Cygni lines become completely independent of τ when τ is large (but not *too* large [see § VI]). We have shown these limiting profiles in Figure 9. In principle, the velocity law can be inferred from such line profiles, but the dependence on velocity is also weak, except near the unreliable line center. Thus, to the extent that an observed profile resembles those in Figure 9, it conveys no information at all.

A fourth caution is that the basic model—spherically symmetric outflow—may be incorrect. Aspect effects in an asymmetric flow can cause systematic changes in the absorption and emission strengths (Cassinelli and Rumpl 1979). Turbulence is a definite possibility, and its existence would vitiate the Sobolev approximation if $v_{\text{turb}} \approx v$. (A small amount of turbulence would have no effect.) The effect of stellar rotation may also be important. The profiles for stellar envelopes with a combination of expansion and rotation have a bewildering variety (Magnan 1970), and such cases are better treated individually.

One indication that all is not well with the simple model is that the absorption trough in the profiles of the strongest lines, e.g., the N v line in ζ Pup, is often observed to be very nearly black over a substantial interval of wavelength, whereas the computed profiles always have a nonzero intensity except just at the violet edge. (This can be seen in Fig. 9.) No combination of optical depth and velocity variation can reduce this residual emission to the observed level. A possible explanation is that the envelope is not spherically symmetric and that we observe the star through the region of greatest density; thus the absorption is large compared with the emission. Even if asymmetry is not the correct explanation of this problem, it no doubt does modify many of the observed profiles.

In addition to our main body of profile calculations, for single lines formed by conservative scattering in an envelope illuminated by white light, we have considered the effects on line formation due to a photospheric absorption profile, collisional excitation, and a second component. We find that collisional excitation is not important in most cases (except for "super stars"). The other two effects can be included *a posteriori* using the fairly simple algorithms we have presented. These algorithms are quite different in effect from the linear superposition that has sometimes been used.

This atlas is intended to aid the interpretation of high-resolution spectra of early-type stars, and its obvious first application is to the catalog of profiles obtained with *Copernicus* and assembled by Snow and Morton (1976). One of the authors (H. J. G. L. M. L.) is currently engaged in such a project in collaboration with T. P. Snow.

This work was supported in part by the National Science Foundation through grant AST 77-23183 to the University of Colorado. H. J. G. L. M. L. was a Visiting Fellow of JILA while this research was being done.

REFERENCES

Abbott, D. C. 1977, Ph.D. thesis, University of Colorado (A).
Barlow, M., and Cohen, M. 1977, *Ap. J.*, **213**, 737 (BC).
Beals, C. S. 1929, *M.N.R.A.S.*, **90**, 202.
———. 1951, *Pub. Dom. Ap. Obs.*, **9**, 1.
Cassinelli, J., Olson, G., and Stalio, R. 1978, *Ap. J.*, **220**, 573.
Cassinelli, J., and Rumpl, W. 1979, in preparation.
Castor, J. I. 1970, *M.N.R.A.S.*, **149**, 111.
———. 1979, in preparation.
Castor, J. I., Abbott, D. C., and Klein, R. I. 1975, *Ap. J.*, **195**, 157 (CAK).
Conti, P. S. 1978, *Astr. Ap.*, **63**, 225.
Conti, P. S., Leep, E. M., and Lorre, J. J. 1977, *Ap. J.*, **214**, 759.
Ebbets, D. C. 1977, Ph.D. thesis, University of Colorado.
Hutchings, J. B. 1970, *M.N.R.A.S.*, **147**, 367.
———. 1977, *Ap. J. (Letters)*, **204**, L99.
Lamers, H. J. G. L. M., and Morton, D. C. 1976, *Ap. J. Suppl.*, **32**, 715 (LM).
Lamers, H. J. G. L. M., and Rogerson, J. B. 1978, *Astr. Ap.*, **66**, 417.
Lamers, H. J. G. L. M., Stalio, R., and Kondo, Y. 1978, *Ap. J.*, **223**, 207.
Lamers, H. J. G. L. M., van den Heuvel, E. P. J., and Petterson, J. A. 1976, *Astr. Ap.*, **49**, 327.
Lucy, L. B. 1971, *Ap. J.*, **163**, 95.
Magnan, C. 1970, *J. Quant. Spectrosc. Rad. Transf.*, **10**, 1.
McCrea, W. H. 1929, *Zs. Phys.*, **57**, 367.
Mihalas, D., Kunasz, P. B., and Hummer, D. G. 1975, *Ap. J.*, **202**, 465.
———. 1976, *Ap. J.*, **210**, 419.
Noerdlinger, P. D., and Rybicki, G. B. 1974, *Ap. J.*, **193**, 651.
Olson, G. 1978, *Ap. J.*, **226**, 124.
Snow, T. P., and Jenkins, E. B. 1977, *Ap. J. Suppl.*, **33**, 269.
Snow, T. P., and Morton, D. C. 1976, *Ap. J. Suppl.*, **32**, 429.
van Regemorter, H. 1962, *Ap. J.*, **136**, 906.

John I. Castor: Joint Institute for Laboratory Astrophysics, University of Colorado, Boulder, CO 80309

Henny J. G. L. M. Lamers: Space Research Laboratory, Beneluxlaan 21, Utrecht, Holland